CHALMERS
UNIVERSITY OF TECHNOLOGY

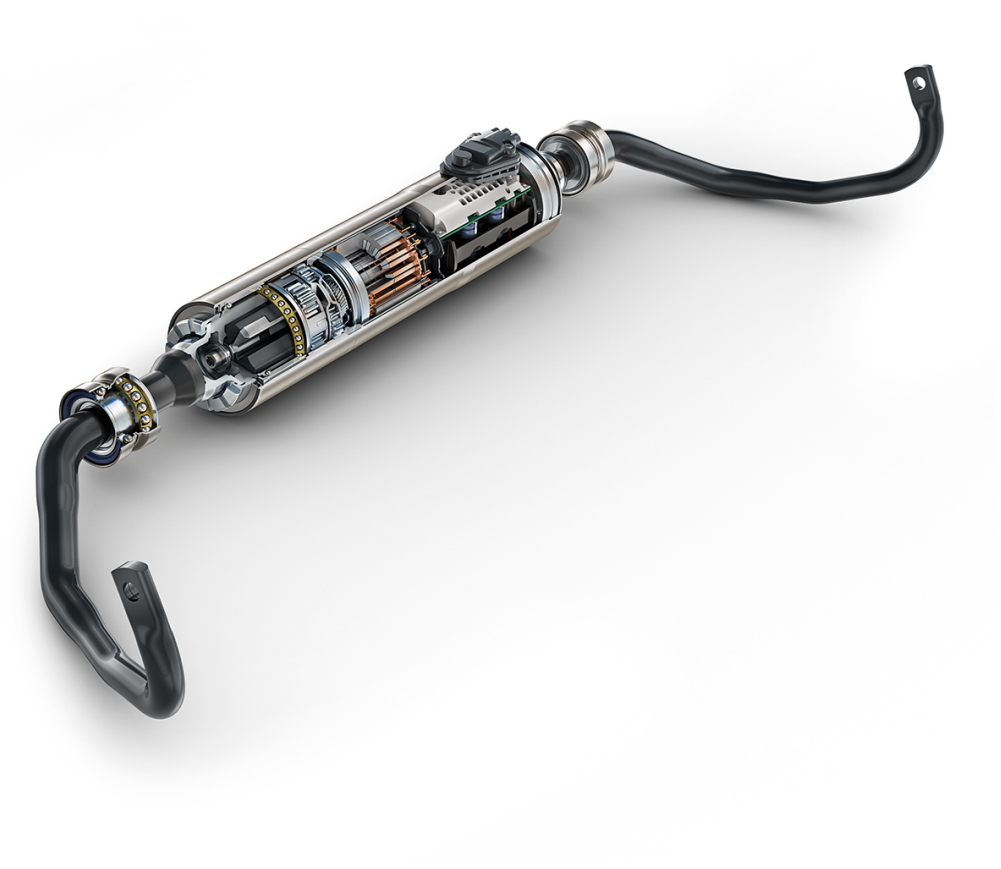

Investigation of active anti-roll bars and development of control algorithm

Master's thesis in Automotive engineering

Harshit Agrawal
Jacob Gustafsson

Department of Applied Mechanics
CHALMERS UNIVERSITY OF TECHNOLOGY
Gothenburg, Sweden 2017

Master's thesis 2017:30

Investigation of active anti-roll bars and development of control algorithm

Harshit Agrawal
Jacob Gustafsson

CHALMERS
UNIVERSITY OF TECHNOLOGY

Department of Applied Mechanics
Division of Vehicle Engineering and Autonomous Systems
Vehicle Dynamics Group
Chalmers University of Technology
Gothenburg, Sweden 2017

Investigation of active anti-roll bars and development of control algorithm
Harshit Agrawal
Jacob Gustafsson

Supervisors: Kristofer Grankvist Park, Volvo Car Corporation
Tushar Chugh, Department of Applied Mechanics
Examiner: Matthijs Klomp, Department of Applied Mechanics

Master's Thesis 2017:30
ISSN 1652-8557
Department of Applied Mechanics
Division of Vehicle Engineering and Autonomous Systems
Vehicle Dynamics Group
Chalmers University of Technology
SE-412 96 Gothenburg
Telephone +46 31 772 1000

Cover: An electromechanical anti-roll bar manufactured by Schaeffler AG, © Schaeffler AG.

Typeset in LaTeX
Printed by Chalmers Reproservice
Gothenburg, Sweden 2017

Investigation of active anti roll bars and development of control algorithm
Harshit Agrawal
Jacob Gustafsson
Department of Applied Mechanics
Chalmers University of Technology

Abstract

Active anti-roll bars have recently found greater acceptance among premium car manufacturers and optimal application of this technology has emerged as an important field of research. This thesis investigates the potential of implementing active anti-roll bars in a passenger vehicle with the purpose of increasing customer value. For active anti-roll bars, customer value is defined in terms of vehicle's ride comfort and handling performance. The objective with this thesis is to demonstrate this value through development of a control algorithm that can reflect the potential improvement in ride comfort and handling.

A vehicle with passive anti-roll bars is simulated for different manoeuvres to identify the potential and establish a reference for the development of a control algorithm and for the performance of active anti-roll bars. While ride is evaluated using single-sided cosine wave and single-sided ramps, handling is evaluated using standardized constant radius, frequency response and sine with dwell manoeuvres.

The control strategy developed implements a combination of sliding mode control, feed forward and PI-controllers. Simulations with active anti-roll bars showed significant improvement in ride and handling performance in comparison to passive anti-roll bars. In ride comfort, the biggest benefit was seen in the ability to increase roll damping and isolating low frequency road excitations. For handling, most significant benefits are through the system's ability of changing the understeer behaviour of the vehicle and improving the handling stability in transient manoeuvres. Improvement in the roll reduction capability during steady state cornering is also substantial.

In conclusion, active anti-roll bars are undoubtedly capable of improving both ride comfort and handling performance of a vehicle. Although the trade-off between ride and handling performance is significantly less, balance in requirements is critical to utilise the full potential of active anti-roll bars. With a more comprehensive control strategy, they also enable the vehicle to exhibit different driving characteristics without the need for changing any additional hardware.

Keywords: Active anti-roll bar, suspension, chassis, vehicle dynamics, handling, ride comfort, roll, yaw, PI-controller, sliding mode controller.

Acknowledgements

First of all, we would like to thank our industrial supervisor Kristofer Grankvist Park for initiating this project and for his support and guidance at Volvo Cars with regular meetings, technical inputs and encouragements. We would also like to express our gratitude to Tushar Chugh for his willingness to help and support especially at the end of the project which was of huge importance for the final results. Furthermore, we would also like thank our examiners, Lars Drugge and Matthijs Klomp for examining the project and giving valuable input during the project. We would also like to thank all the great people we met at Volvo Cars for their warm welcome and support with a special mention to our department, Wheel Suspension, tuning & Active suspension and the vehicle dynamics department. A special thanks also to Pontus Carlsson for enduring our questions related to control strategies and David Andersson, Mohit Hemant Asher, Alejandro Gonzalez, Catharina Hansen for their support with simulation software packages.

Finally, we would like to thank our family and friends for their valuable encouragements and support during the project.

Jacob Gustafsson & Harshit Agrawal, Gothenburg, June 2017

Nomenclature

Symbols

C	Cornering Stiffness $[N/rad]$
F	Force $[N]$
F_y	Lateral Force $[N]$
G_{ref}	Roll reference gain [-]
$H(S)$	Transfer function [-]
I_{xx}	Moment of inertia around the x-axis $[kgm^2]$
I_{zz}	Moment of inertia around the z-axis $[kgm^2]$
K	Gain for the sliding mode controller [-]
K_D	Derivative gain for a PID controller [-]
K_I	Integral gain for a PID controller [-]
K_P	Proportional gain for a PID controller [-]
K_{us}	Understeer coefficient $[rad/m/s^2]$
L	Wheelbase $[m]$
M_z	Additional moment induced around the z-axis $[Nm]$
S	Sliding surface of SMC [-]
a_y	Lateral acceleration $[m/s^2]$
b	Distance from CoG to rear axle $[m]$
c_{FD}	Front damper constant $[Ns/m]$
c_{RD}	Rear damper constant $[Ns/m]$
e	Tuning parameter for the sliding mode controller [-]
f	Distance from CoG to front axle $[m]$
g	Gravitational acceleration $[m/s^2]$
h_{RC}	Roll centre height $[m]$
i	Motion ratio [-]
k_{FS}	Front spring stiffness $[N/m]$
k_{RS}	Rear spring stiffness $[N/m]$
k_z	Vertical stiffness $[N/m]$
k_γ	Torsional stiffness $[Nm/rad]$
k_φ	Roll stiffness $[Nm/rad]$
m	Mass $[kg]$
r_{ARB}	Length of anti-roll bar arm $[m]$
s	Complex frequency [-]
t	Time [sec]
v_x	Longitudinal velocity $[m/s]$
v_y	Lateral velocity $[m/s]$
w	Track width $[m]$
y_1	1^{st} order sliding surface of SMC [-]
y_2	2^{nd} order sliding surface of SMC [-]
z	Vertical displacement $[m]$
Δh	Distance from CoG to roll centre $[m]$
δ	Average steer angle at wheels $[rad]$
δ_{SW}	Steering wheel angle $[deg]$

γ	Torsion angle $[rad]$
ω_0	Eigenfrequency $[Hz]$
φ	Roll angle $[rad]$
$\dot{\varphi}$	Roll rate $[rad/s]$
$\ddot{\varphi}$	Roll acceleration $[rad/s^2]$
$\dot{\psi}$	Yaw rate $[rad/s]$
$\ddot{\psi}$	Yaw acceleration $[rad/s^2]$
ζ	Damping ratio [-]

Subscripts

ARB	At anti-roll bar
ARB,w	From anti-roll bar on wheel
F	Front
FARB	At front anti-roll bar
FL	Front left
FR	Front right
R	Rear
RARB	At rear anti-roll bar
RL	Rear left
RR	Rear right
ref	Reference
w	At wheel

Abbreviations

1D	One Dimensional
ABS	Anti-lock Braking System
ARB	Anti-Roll Bar
CoG	Centre of Gravity
ESC	Electronic Stability Control
FARB	Front anti-roll bar
ISO	International Organization for Standardization
NHTSA	National Highway Traffic Safety Administration
OEM	Original Equipment Manufacturer
ORV	Overall Ride Value
PSD	Power Spectral Density
RARB	Rear anti-roll bar
RDNA	Ride DNA
RMS	Root Mean Square
SMC	Sliding Mode Control
SWA	Steering Wheel Angle

Contents

List of Figures

List of Tables

1
Introduction

1.1 Background

The competitive premium car segment forces car manufacturers to look for alternative techniques to increase customer value. Old concepts are reviewed to find areas for improvement and there is a need for implementation of new technologies. One of these areas is the anti-roll bar.

An anti-roll bar (ARB) or a stabilizer bar, as it also called, is a component in the suspension of most vehicles today. An ARB is commonly a metal bar whose ends are connected to the left and right suspensions systems. The purpose with the ARB is to increase the vehicle's roll stiffness without the need of altering the stiffness of the springs in the suspension. During body roll the left and right wheel will be displaced in opposite directions. This gives rise to twisting in the ARB which creates a counteracting moment on the body, reducing body roll. In a case were both the left and right wheel, on one axle, are simultaneously displaced in the same direction, for example in pure pitch motion, the ARB will not generate any forces. However, the anti-roll bars ability to reduce roll of the vehicle has a side effect. If one of the wheels would hit a obstacle such as a pothole then this will induce torsion of the ARB and hence both wheels will be effected in such a situation, this is often referred to as the copying effect. This gives a higher negative impact on ride comfort compared to if the two wheels could move independently of each other. To reduce this trade-off active ARBs, i.e. ARBs with variable stiffness, are considered. [1].

The first active ARB used in production vehicles was introduced in the 1995 year model Citroen Xantia Activa. That was a hydraulic ARB that consisted of a passive ARB with hydraulic ARB links, i.e. the connection between the ARB and the mounting point to the suspension system. [2]

Ten years later Aisin Seiki Co, in cooperation with Toyota, developed an electromechanical ARB to reduce the energy consumption, improve steering feel and reduce the actuator volume compared to the hydraulic systems [3]. This electromechanical ARB was introduced for the first time in Lexus GS 430 in year 2005 [4].

Since 2005 the technology have been further developed and today an increase in usage of electromechanical anti-roll bars is seen within the industry, for example BMW using electromechanical anti-roll bars in their 7-series [5]. This thesis aims at investigating the possible benefits of implementing an electromechanical anti-roll bar in today's cars and how they can be used to increase customer value.

1.2 Objectives

The objective with this thesis is to investigate how active anti-roll bars can be used to improve customer value. A control algorithm shall be developed for a particular electromechanical anti-roll bar and the impacts on ride comfort and handling is to be evaluated. These properties shall be evaluated through objective testing in an offline simulation environment.

1.3 Delimitations

The focus of this thesis is limited to the theoretical and vehicle dynamics aspects of using active anti-roll bars and development of an ideal control strategy. Hence the practical aspects such as packaging studies and cost is out of the scope of this thesis. The following additional limitations are made in conjunction with Volvo Cars:

- The active anti-roll bar is only implemented on the Volvo XC90, other models will not be studied.
- The control strategy developed is to be ideal, i.e. no consideration will be taken to signal delays or limitations of the existing electrical architecture of the XC90.
- The control strategy is developed for simulations and not developed for a target ECU and not tested in a real vehicle. Hence problems with input signal quality and run time will not be solved.
- Evaluation of active anti-roll bars will only be conducted for the case with both front and rear axle equipped with electromechanical anti-roll bars.
- The active anti-roll bar to be used in this project is a given electromechanical anti-roll bar manufactured by a given company. The hardware for the active anti-roll bars is considered to be a given and will not be studied in detail.
- The active anti-roll bar will be considered as a standalone system and for this proof of concept and will not be implemented together with other active functions e.g. active dampers.
- Meeting safety standards and failure mode analysis are not strictly part of the scope. Certain safety aspects will still need to be considered in order to obtain a robust control system.

2
Theory

This chapter explains the physics of an ARB and the mathematics of how an ARB affects the vehicle. Furthermore customer value is characterised in terms of ride comfort and handling. These two concepts are also explained and put in the context of ARBs. Finally, the existing active ARB concepts are presented and explained.

2.1 Passive anti-roll bars

Passive ARBs are the most commonly used ARB in vehicles today. A passive ARB is often a metal bar bent into roughly a U-shape. The exact shape is often complex due to packaging reasons even though an optimal ARB is one with as few bends as possible [1].

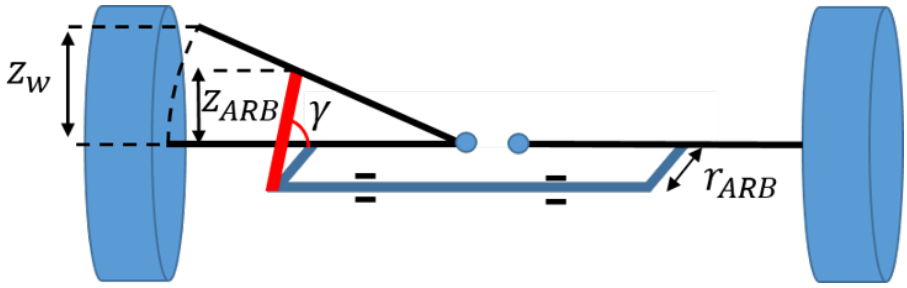

Figure 2.1: A simple U-shaped ARB. The red line represents the ARB when subject to the vertical wheel displacement z_w which induces the torsion angle γ.

The torsional stiffness of the ARB, its geometry and attachment point to the chassis is what defines its ability to counteract roll motion. For simplicity the ARB, in this thesis, is considered to be strictly U-shaped, see Figure 2.1. Furthermore the concept of motion ratio is used to account for the difference in vertical motion between the wheel z_w and the studied component, in this case the ARB z_{ARB}. This difference occurs due to the suspension kinematics, the position of the ARB and its orientation [1]. The motion ratio i_{ARB} relates the vertical motions and corresponding forces according to equation 2.1.

$$i_{ARB} = \frac{z_{ARB}}{z_w} = \frac{F_{ARB,w}}{F_{ARB}} \tag{2.1}$$

In equation 2.1, F_{ARB} is the force produced at each of the two ARB ends and $F_{ARB,w}$ is the corresponding forces acting on the wheel. The ARB is assumed to have a torsional stiffness k_γ and an arm length r_{ARB}. The function of the ARB can be exemplified by exciting the left wheel according to Figure 2.1 while the right wheel is kept stationary. This results in a torsion in the ARB which induces forces at the ARB ends acting on the wheels. The corresponding force acting on each wheel $F_{ARB,w}$ is determined using equation 2.2. Note that by substituting the product between the torsional stiffness k_γ and the torsion angle γ with the torque produced by the ARB, T_{ARB}, enables use of the same equation for a non conventional ARB.

$$F_{ARB,w} = \frac{k_\gamma \gamma}{2r_{ARB}} i_{ARB} = \frac{T_{ARB}}{2r_{ARB}} i_{ARB} \tag{2.2}$$

2.2 Ride comfort

Ride comfort is a term that is hard to define. Griffin [6] states that there are several factors contributing to the overall comfort, among others the term vibrational discomfort. Individual variations are also said to be of great importance to how comfort is perceived, hence it is hard to quantify comfort and the effect of the individual contributing factors.

In the automotive industry the concept ride comfort is often divided into three main parts; vibrations, harshness and noise. The division is based on the frequency ranges, as shown in Figure 2.2. Frequencies from 0.1-20Hz is called tactile oscillations or vibrations, 100Hz and above is called audible oscillations or noise and in-between these two there is a transition zone referred to as harshness. [1].

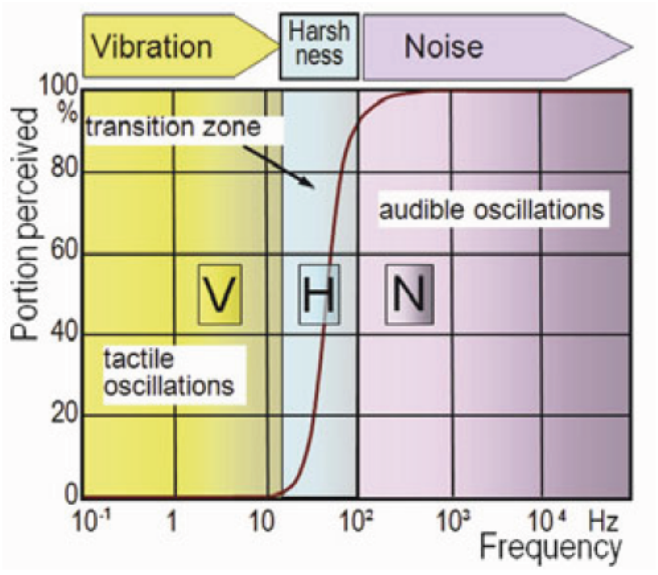

Figure 2.2: Three phenomena which are usually considered to be part of the ride comfort in the automotive industry [1].

In this thesis focus is put on the tactile oscillations and the lower region of the transition zone. Furthermore this area is commonly divided into primary and secondary ride. The primary ride is vibrations with low frequencies and secondary ride is vibrations with higher frequencies. Here everything under 3Hz is considered primary ride and above 3Hz is considered to be secondary ride.

The relationship between vibrations and discomfort is well determined in research. ISO 2631-1 [7] is a commonly used standard that describes how to quantify the influence from vibrations on the perceived discomfort for frequencies in the range 1-80Hz. This is done by frequency weighted RMS values of accelerations [7]. The reason for frequency based weighting is to take into account that the human body is more sensitive to certain frequencies. Dieckmann [8] shows that frequencies below 1Hz gives rise to motion sickness and frequencies of 4-5Hz are the resonance frequencies for whole body movements and around 20-25Hz are the resonance frequencies of the head and neck. These results are also supported by ISO 2631-1 [7] but they extend the 4-5Hz interval presented by Dieckmann to a 4-8Hz interval where the human is considered to be the most sensitive to vibrations.

Guglielmino et.al [9] states that the major source of vibrations in a vehicle is road irregularities and Senthil Kumar et.al [10] states that a good way of comparing the ride between vehicles is comparing overall ride values (ORV). ORV is defined as the sum of the weighted RMS values. Using this methodology, based on ISO 2631-1997 and the British vibration standard BS 68441-1987 they conclude that the principal sources of discomfort is vertical vibrations at the seat and feet and fore & aft vibrations at the seatback. Furthermore it is concluded that the contributions of rotational accelerations to the overall ride values can be ignored.

However, Ibicek et.al [11] shows that vehicle roll also influences the perception of discomfort. By placing a vehicle on a four post-rig human subjects were exposed to roll movement's measured in RMS values of the roll acceleration and asked to rate their level of discomfort. It was shown that the discomfort level increased with the RMS values of the acceleration in the studied range, $0 - 0.6\text{m/s2}$. These results are also supported by Guglielmino et.al [9] who states that a higher roll centre is perceived as more comfortable than a low roll centre. Furthermore Koumura et.al [12] have shown that for a certain vehicle the resonance frequency for roll accelerations is around 2Hz and that a second peak exists around 5Hz. These frequencies are in the range close to the natural frequencies of the human body and hence it can be concluded that the roll is of importance for the perceived discomfort.

The roll acceleration gain has been determined to be primarily dependent on the roll stiffness and the roll-damping coefficient. Around the resonance frequency Koumura et.al [12] has shown that an increase in roll stiffness increases the roll response while an increase in roll-damping decreases the roll response.

2.2.1 Half car model

A half car model with a roll center can be used to describe a vehicles roll dynamics, see Figure 2.3.

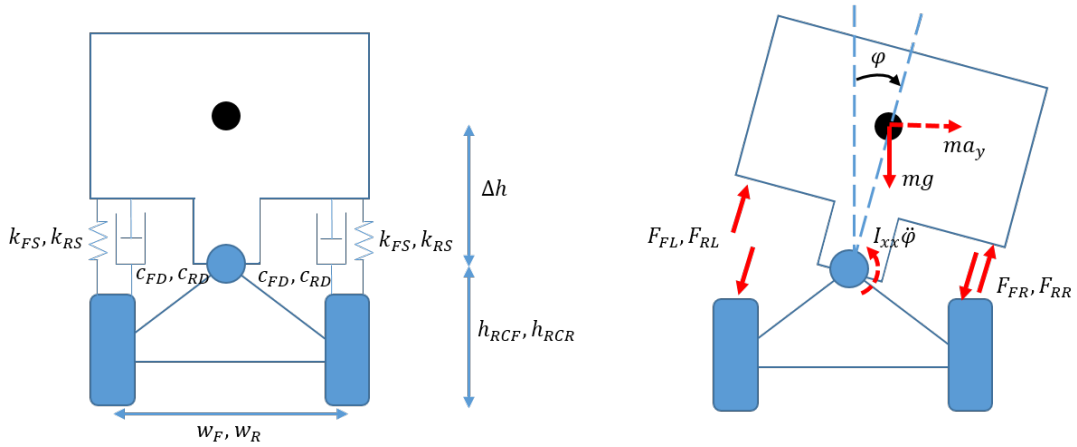

Figure 2.3: Illustration of a half car model with a roll center, subject to a lateral acceleration of a_y which gives rise to the body roll angle φ.

Moment equilibrium around the roll centre for the car body results in equation 2.3. Note that the equation is derived with the assumption that the body roll angle φ is small.

$$RC : ma_y\Delta h + mg\Delta h\varphi + \frac{w_F}{2}(F_{FL} - F_{FR}) + \frac{w_R}{2}(F_{RL} - F_{RR}) = I_{xx}\ddot{\varphi} \tag{2.3}$$

By geometry and assuming that the torsion angle γ is a small angle, the relation between roll angle φ and torsion angle for the front γ_F respectively rear axle γ_R can be determined, see equation 2.4.

$$\gamma_F = \frac{w_F i_{FARB}}{r_{FARB}}\varphi \tag{2.4a}$$

$$\gamma_R = \frac{w_R i_{RARB}}{r_{RARB}}\varphi \tag{2.4b}$$

Using equation 2.4, to substitute the torsion angle, expressions for the forces from the suspension acting on the chassis are obtained, see equation 2.5. All forces from the suspension are assumed to be acting along the normal to the car body.

$$F_{FL} = -k_{FS}i_{FS}^2\frac{w_F}{2}\varphi - k_{z,FARB}i_{FARB}^2\frac{w_F}{2}\varphi - c_{FD}i_{FD}^2\frac{w_F}{2}\dot{\varphi} \tag{2.5a}$$

$$F_{FR} = k_{FS}i_{FS}^2\frac{w_R}{2}\varphi + k_{z,FARB}i_{FARB}^2\frac{w_R}{2}\varphi + c_{FD}i_{FD}^2\frac{w_R}{2}\dot{\varphi} \tag{2.5b}$$

The forces for the rear axle are determined in the exact same way as for the ones for the front axle. Inserting these forces in equation 2.3 results in equation 2.6.

$$I_{xx}\ddot{\varphi} = ma_y\Delta h + mg\Delta h\varphi - k_{\varphi,FS}\varphi - k_{\varphi,FARB}\varphi - c_{\varphi,FD}\dot{\varphi} - k_{\varphi,RS}\varphi - k_{\varphi,RARB}\varphi - c_{\varphi,RD}\dot{\varphi} \tag{2.6}$$

The roll stiffness k_φ and damping c_φ for the front and rear axle are defined according to equation 2.7.

$$k_{\varphi,FS} = k_{FS}i_{FS}^2\frac{w_F^2}{2} \tag{2.7a}$$

$$k_{\varphi,FARB} = k_{z,FARB}i_{FARB}^2\frac{w_F^2}{2} \tag{2.7b}$$

$$c_{\varphi,FD} = c_{FD}i_{FD}^2\frac{w_F^2}{2} \tag{2.7c}$$

$$k_{\varphi,RS} = k_{RS}i_{RS}^2\frac{w_R^2}{2} \tag{2.7d}$$

$$k_{\varphi,RARB} = k_{z,RARB}i_{RARB}^2\frac{w_R^2}{2} \tag{2.7e}$$

$$c_{\varphi,RD} = c_{RD}i_{RD}^2\frac{w_R^2}{2} \tag{2.7f}$$

Taking the Laplace transform of equation 2.6 makes it possible to determine a transfer function from the lateral acceleration a_y to the roll angle φ. The transfer function can be written on the general form shown in equation 2.8.

$$\frac{\varphi(s)}{a_y(s)} = \frac{\varphi(s)}{a_y(s)}_{static} \cdot \frac{1}{s^2 + \frac{2\zeta}{\omega_0}s + \frac{1}{\omega_0^2}} \tag{2.8}$$

The first term in equation 2.8 describes the stationary behaviour of the vehicle. This is often referred to as the steady state roll gradient of a vehicle. The general roll gradient is expressed in equation 2.9

$$\frac{\varphi(s)}{a_y(s)}_{static} = \frac{m\Delta h}{-mg\Delta h + k_{\varphi,FS} + k_{\varphi,FARB} + k_{\varphi,RS} + k_{\varphi,RARB}} \tag{2.9}$$

The dynamic part of the transfer function is defined by the damping ratio ζ determining the damping and the eigenfrequency ω_0. The damping ratio and eigenfrequency are determined in equation 2.10

$$\zeta = \frac{c_{\varphi,FD} + c_{\varphi,RD}}{2\sqrt{I_{xx}}\sqrt{-mg\Delta h + k_{\varphi,FS} + k_{\varphi,FARB} + k_{\varphi,RS} + k_{\varphi,RARB}}} \tag{2.10a}$$

$$\omega_0 = \sqrt{\frac{-mg\Delta h + k_{\varphi,FS} + k_{\varphi,FARB} + k_{\varphi,RS} + k_{\varphi,RARB}}{I_{xx}}} \tag{2.10b}$$

Comparing the results from equation 2.8 to 2.10 with the theory presented in section 2.2 it can be concluded that both shows the same behaviour. An increase in roll stiffness reduces damping and an increase in damper constants increases the roll damping and vice verse. Furthermore, increased roll stiffness increases the roll eigenfrequency and reduces the static roll gradient.

2.3 Handling

The amount of lateral load transfer that occurs between two wheels of an axle has a significant influence on vehicle's lateral or handling dynamics. During a manoeuvre, the change in lateral stiffness of left and right wheels are not equal in magnitude due to the non-linear characteristics of tyres. This behaviour results in a net decrease in lateral stiffness of the axle during corners and is proportional to the amount of load transfer. Figure 2.4 shows the relationship between lateral stiffness and vertical load for a particular tyre.

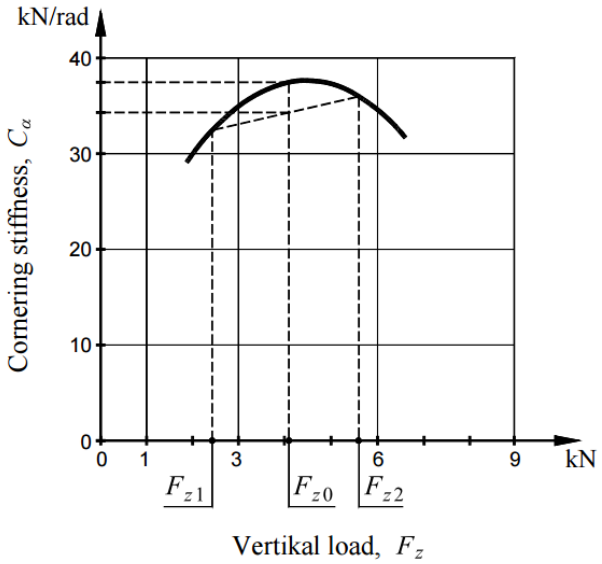

Figure 2.4: Cornering stiffness, C_α, as a function of vertical load, F_z, for Michelin ZX 155 SR 14. F_{z0} is vertical load at equal tyre load. F_{z1} and F_{z2} corresponds to a load transfer of 1500 N [13].

By allowing variable stiffness of ARB in front and rear axle, the respective load transfer and thus, the lateral stiffness can be manipulated to achieve the desired handling characteristics of the car. The ability to vary stiffness on both axles can allow the vehicle to achieve the desired lateral characteristics whilst also following the target roll behaviour.

Vehicle roll has a direct influence on handling characteristics as well, through roll steer and can be influenced by ARBs. During a manoeuvre, jounce/rebound motion of suspension causes the outer wheels of the front axle to steer further outwards (toe-out) and the inner wheel to steers inwards (toe-in). On the rear axle, the outer wheel undergoes toe-in and the inner wheel undergoes toe-out. These behaviour create an understeering effect [13]. By reducing roll of a vehicle, the amount of understeer is reduced which in turn reduces the required steering angle. Figure 2.5 shows the toe angle change for a typical McPherson suspension. For actual toe-angle variation, refer Appendix B.1.

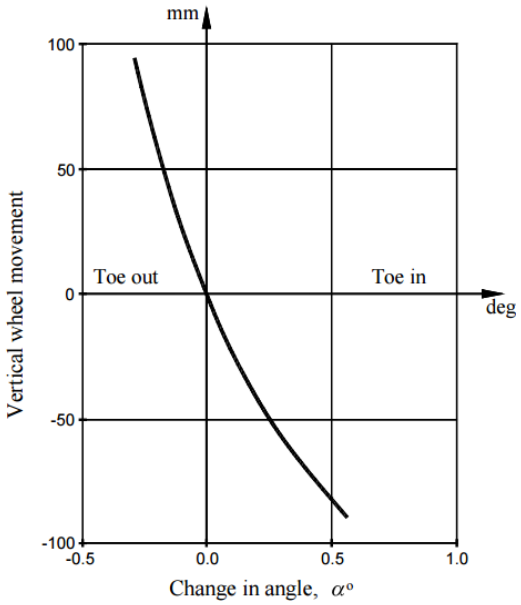

Figure 2.5: Toe-in change at jounce and rebound for a McPherson suspension [13].

2.3.1 Bicycle model

Bicycle model (also referred to as single track model) is the most commonly used model for defining lateral and yaw dynamics of a vehicle. It is a linear 2-DOF model which makes certain assumptions to simplify calculations. The most important assumptions are:

- Front and rear axles represented by one tyre each
- No lateral and longitudinal load transfer
- No roll and pitch motion
- Longitudinal velocity is constant
- Small slip angles, i.e. tyres operate in linear stiffness range

A typical bicycle model is represented in Figure 2.6.

Force equilibrium equations for bicycle model are presented in equations 2.11 to 2.13.

$$m(\dot{v_x} - \dot{\psi}v_y) = -F_{y,F}sin(\delta) \tag{2.11}$$

$$m(\dot{v_y} + \dot{\psi}v_x) = F_{y,R} + F_{y,F}cos(\delta) \tag{2.12}$$

$$I_{zz}\ddot{\psi} = fF_{y,F}cos(\delta) - bF_{y,R} \tag{2.13}$$

Here,

$F_{y,F}$ is the lateral force on the front axle
$F_{y,R}$ is the lateral force on the rear axle
δ is the average steering angle of the front wheels

Based on the small slip-angle assumption, lateral forces $F_{y,F}$ and $F_{y,R}$ can be defined as linear functions of the slip angle, as shown in equation 2.14.

$$F_{y,F} = -C_F\alpha_F \tag{2.14a}$$

$$F_{y,R} = -C_R\alpha_R \tag{2.14b}$$

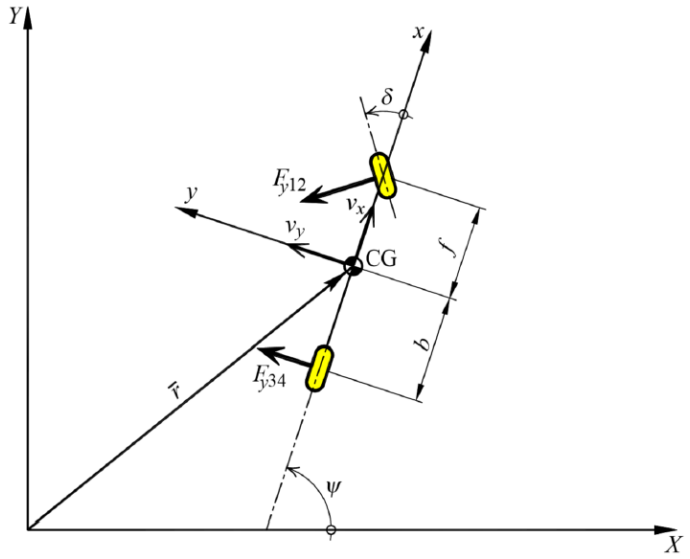

Figure 2.6: Bicycle Model [13]. The notation 12 is substituted for F and 34 is substituted for R.

In equation 2.14,

C_F and C_R	are the cornering stiffness of the front and rear axle respectively
α_F and α_R	are the lateral slip angle on the front and rear axle respectively

Slip angles can be further expressed as functions of lateral and longitudinal velocities, as shown in equation 2.15 .

$$\alpha_F = \arctan\left(\frac{v_y + \dot{\psi} f}{v_x}\right) - \delta \tag{2.15a}$$

$$\alpha_R = \arctan\left(\frac{v_y - \dot{\psi} b}{v_x}\right) \tag{2.15b}$$

Substituting equations 2.14 and 2.15 into equations 2.12 and 2.13, state space equations are obtained for the bicycle model, see equation 2.16.

$$\begin{bmatrix} \frac{C_F + C_R}{v_x} & mv_x + \frac{fC_F - bC_R}{v_x} \\ \frac{fC_F - bC_R}{v_x} & \frac{f^2 C_F + b^2 C_R}{v_x} \end{bmatrix} \begin{bmatrix} v_y \\ \dot{\psi} \end{bmatrix} + \begin{bmatrix} m\dot{v}_y \\ I_{zz}\ddot{\psi} \end{bmatrix} = \begin{bmatrix} C_F \\ fC_F \end{bmatrix} \delta \tag{2.16}$$

2.3.2 Yaw Dynamics

In yaw dynamics, the ideal vehicle state is the steady state, i.e. lateral acceleration and yaw rate are constant. Using steady state conditions in equation 2.16, an expression for yaw rate of the vehicle is obtained, see equation 2.17.

$$\frac{\dot{\psi}}{\delta} = \frac{v_x L C_F C_R}{L^2 C_F C_R + m v_x^2 (b C_R - f C_F)} \tag{2.17}$$

The expression in 2.17 is also referred to as steering sensitivity. Due to the non-linear behaviour of the tyre stiffness, estimation of vehicle's cornering stiffness is not always accurate. Therefore, it is desirable to define handling characteristics of car on basis of only those quantities that can be easily logged in a vehicle such as steering angle and lateral acceleration. Rearranging the equation 2.17, the expression in equation 2.18 is obtained.

$$\dot{\psi} = \frac{v_x}{L + v_x^2 K_{us}} \delta \tag{2.18}$$

Where, K_{us} is the understeer coefficient and is expressed as per equation 2.19.

$$K_{us} = \frac{m(b C_R - f C_F)}{L C_F C_R} \tag{2.19}$$

As can be seen in 2.19, K_{us} is only dependent on vehicle properties. Using the observations in 2.20, equation 2.18 can be rearranged to equation 2.21 for steady state.

$$\dot{\psi} = v_x / R \tag{2.20a}$$
$$a_y = v_x^2 / R \tag{2.20b}$$

$$\delta = L/R + K_{us} a_y \tag{2.21a}$$
$$\delta_{K_{us} \to 0} = L/R \tag{2.21b}$$

For a K_{us} value of zero, the vehicle is said to be neutral steered. For negative values of K_{us}, the required steering angle is lower than in steady state conditions and thus, the vehicle has an oversteering behaviour. For positive values, as the steering angle is larger, the vehicle is understeered. Therefore, in terms of simplicity, understeer coefficient is the preferred quantity for defining handling characteristics of a vehicle.

2.4 Active anti-roll bars

As some of the requirements for achieving good handling characteristics are contradictory to those required for ride, a compromise must be made in order to achieve a reasonable ride-handling balance. This trade-off is engineered mostly by varying body stiffness, suspension tuning and anti-roll bars. While body stiffness is a passive component, extensive research has been done on active suspension and the technology is successfully implemented in most premium cars today. However, the amount of research on development in active ARB has been relatively lacking. Earliest active ARB systems were hydraulic and until recently, they have been the predominant choice over electromechanical systems.

Active ARB systems provide the ability to vary the effective stiffness of the chassis and thus, reducing the amount of trade-off required in balancing ride and handling characteristics. Supported by suitable actuator control for ARB, the chassis can be made stiffer to provide better agility during cornering or made softer in rough road conditions to improve ride comfort characteristics.

2.4.1 Hydraulic anti-roll bars

The first application of hydraulic ARBs on a production car was seen in 1995 by Citroen in Xantia Activa. Several rotary and linear-actuator based systems have been developed since then. Use of hydraulic systems have been limited due to some obvious drawbacks like [14]:

- Requirement for dedicated hydraulic components like supply lines, control unit, valves etc. and their associated cost
- Additional power requirements for hydraulic pump and impact on fuel efficiency
- Relatively poor frequency response
- Maintenance requirements on the hydraulic components

2.4.2 Electromechanical anti-roll bars

The concept of electromechanical ARBs is essentially the same as for passive ARBs, but instead of letting the torsion dictate the torque produced by the ARB, any torque can be requested at any time. Electromechanical ARBs can be understood as two halves of passive ARB connected to each other via an electric motor and a gearbox. Therefore, the motor dictates the anti-roll bar torque. The control signal sent to the motor, which determines the output torque, is often created by a controller built in to the active ARB. In most cases this controller also takes disturbances into account and tries to follow the inputted desired torque value. Figure 2.7 illustrates the working concept of electromechanical ARBs.

The first application of electric ARB system was carried out by Toyota in cooperation with Aisin Seiki Co. for the 2005 Lexus G430 [4]. Only recently, there has been substantial increase in application of electromechanical roll control systems with OEMs like Bentley [15], Porsche [16], Audi [17] and BMW [18] implementing this technology in their premium cars.

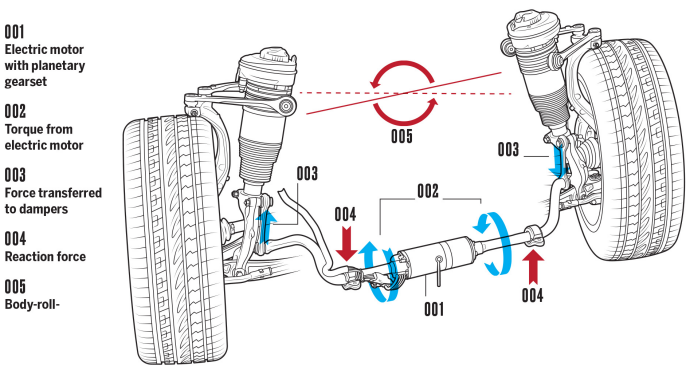

Figure 2.7: Concept behind electro-mechanical ARBs [19].

Electromechanical ARB systems fare much better than hydraulic systems by reducing the impact on fuel efficiency and enabling easier integration and maintenance [14]. Electromechanical anti-roll bars developed by Schaeffler Group (Schaeffler Technologies AG & Co. KG) are currently the most widely used active ARBs.

2.5 Control theory

Controlling the behaviour of the active ARB can be done in several different ways. This section explains the theory behind the different controllers implemented in this thesis and the active ARB plant model the controllers are to control.

2.5.1 Active anti-roll bar plant model

As a substitute for the physical electromechanical active ARB studied, a Simulink based s-function replicating its behaviour is used in simulations. This plant model is developed and tested by the supplier and hence the exact properties of this plant is unknown and the plant model is in this thesis treated as a black box.

However the inputs and outputs from the plant model are known. The input is a desired torsion angle and disturbances derived from wheel motions. The output from the plant model is the delivered actuator torque which is related to wheel forces according to equation 2.2. The second output is the actual torsion angle of the anti-roll bar. In the ideal case the inputted torsion angle is proportional to the torque output with the stiffness of the system hence the input can be seen as a desired torque divided by the system stiffness.

As the plant model replicates a real physical ARB it is far from ideal. Understanding the basic functionality of the ARB plant model is necessary to understand the possible implications it can have on the overall system performance. The first and most important non-linearity of the plant model is the limitation of the output torque. The actuator is only able to produce a certain maximum torque output. Furthermore from a frequency sweep it can be seen that this maximum torque output decays with increased frequency, i.e. the bandwidth of the controller is frequency dependent. Lastly, the friction within the actuator is also modelled and hysteresis effects can occur which further increases the non-linearity of the plant model.

2.5.2 PID controller

PID controller is a commonly used controller in industrial applications. Its name comes from how it uses a feedback signal and based on the error between the feedback and the setpoint determines the control signal. Namely it uses a proportional part, the integral of the error and the derivative of the error. A general control scheme for a arbitrary plant controlled by a PID is shown in Figure 2.8.

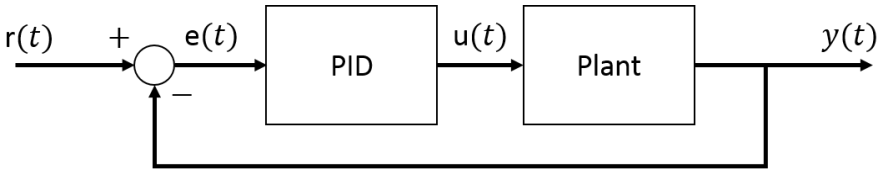

Figure 2.8: A typical application of a PID controller. Based on the error $e(t)$, i.e. the difference between the reference $r(t)$ and the output $y(t)$, a control signal $u(t)$ is sent to the plant, which is representing the system that is controlled.

Understanding how the PID controller affects the plant is a key to choose the right parameter to control. This can be illustrated by applying a PID controller to the system described in equation 2.6, i.e. in this example the plant model is considered to be the vehicle. By transforming this equation into the Laplace domain equation 2.22 is obtained.

$$\begin{aligned} I_{xx}s^2\varphi(s) + (c_{\varphi,FD} + c_{\varphi,RD})s\varphi(s) + \\ (-mg\Delta h + k_{\varphi,FS} + k_{\varphi,RS})\varphi(s) = ma_y(s)\Delta h \end{aligned} \tag{2.22}$$

Introducing a PID controller with the gains K_P, K_I and K_D, the corresponding control signal created by the controller in the Laplace domain is expressed in equation 2.23.

$$u(s) = (K_P + K_I\frac{1}{s} + K_Ds)e(s) \tag{2.23}$$

In equation 2.24 a PID controller is applied to minimise the roll rate $\dot{\varphi}$, i.e. the setpoint is set to zero. The active ARB plant is in this case simplified to be ideal, i.e. it is represented by a simple stiffness $k_{\varphi,AARB}$ without delays and the inbuilt controller is not considered.

$$\begin{aligned} I_{xx}s^2\varphi(s) + (c_{\varphi,FD} + c_{\varphi,RD})s\varphi(s) + (-mg\Delta h + k_{\varphi,FS} + k_{\varphi,RS})\varphi(s) + \\ k_{\varphi,AARB}(K_P + K_I\frac{1}{s} + K_Ds)s\varphi(s) = ma_y(s)\Delta h \end{aligned} \tag{2.24}$$

Rewriting equation 2.24 yields in equation 2.25. From this it can be seen that applying a PID controller on roll rate not only increases the damping in the system it also increases the inertia through the derivative part and the stiffness through the integral part.

$$\begin{aligned} (I_{xx} + K_Dk_{\varphi,AARB})s^2\varphi(s) + (c_{\varphi,FD} + c_{\varphi,RD} + K_Pk_{\varphi,AARB})s\varphi(s) + \\ (-mg\Delta h + k_{\varphi,FS} + k_{\varphi,RS} + K_Ik_{\varphi,AARB})\varphi(s) = ma_y(s)\Delta h \end{aligned} \tag{2.25}$$

2.5.3 Sliding mode control

Different components of a vehicle such as tyres, springs and dampers rarely exhibit linear behaviour. Because of the limitations of the bicycle model, non-linearities like lateral load transfer and cornering stiffness are not modelled and it becomes necessary to employ a control strategy that can account for these behaviours instead. It is particularly important when modelling ARBs as the major influence of ARB is due to the control of lateral load transfer in a vehicle.

Sliding Mode Control, or SMC, is a control strategy commonly implemented with non-linear plants. The non-linear characteristics of the SMC are the result of the control law which relies only on dynamics of error and is independent of the plant. Thus, this strategy is particularly useful when the exact representation of the plant is unknown, as in the case of active ARB plant model introduced in section 2.5.1. The SMC strategy is also a robust solution as it helps in avoiding plant linearization and approximation generally associated with using control strategies that are dependent on the plant. These benefits provide a distinct advantage over the PID control strategy as the tuning of a non-linear controller for different operating conditions becomes potentially easier.

Shtessel, et al. [20] presents the possibility of implementing SMC in vehicle stability applications. A yaw-rate based observer is proposed based on a non-linear vehicle model that can be employed in ABS.

SMC attempts to control a system by constantly adjusting itself (or 'sliding') along a boundary condition i.e. a 'sliding surface'. Boundary condition is essentially the zero error condition where definition of the error varies depending on the application of the controller. Two broad categories of SMC exist, classical sliding mode control (or first-order SMC) and second-order SMC.

While classical sliding mode controller provide a robust control, they are seldom used. It is mainly because of their tendency to produce high frequency switching in the control signal, also referred to as chattering effect. This effect is completely unacceptable for systems with physical implications. Second order SMC solves the chattering issue by using the second order time derivative of the sliding surface instead of the first order [20].

Canale, et al. [21] implements the sub-optimal type of a second order SMC for vehicle yaw control on active differential. The controller is based on a steady state single-track vehicle model and the results achieved are indicative of the controller's potential in improving vehicle handling characteristics. As the requirements for this thesis are similar, an attempt is made to employ sub-optimal controller for yaw control using active ARBs. The general expression for a sub-optimal second order SMC is given in equation 2.26.

$$\dot{y_1}(t) = \dot{S}(t) = y_2(t) \tag{2.26a}$$

$$\dot{y_2}(t) = \ddot{S}(t) = \lambda(t) + \tau(t) \tag{2.26b}$$

Here, S refers to the boundary condition or the sliding surface. λ and τ are bounded functions of which τ is a function of the control variable and is defined using the sub-optimal control law, as explained later in the section.

In the application of lateral dynamics control, the objective is to follow a reference yaw rate. Therefore, the boundary condition is based on yaw rate error, see equation 2.27.

$$S = \dot{\psi} - \dot{\psi}_{ref} \tag{2.27}$$

Using equation 2.27 and moment equilibrium equations for a vehicle, equation 2.26 can be rewritten as equation 2.28.

$$\dot{y_1}(t) = \dot{S}(t) = \frac{fF_{y,F} - bF_{y,R} + M_z(t)}{I_{zz}} - \ddot{\psi}_{ref} \tag{2.28a}$$

$$\dot{y_2}(t) = \ddot{S}(t) = \underbrace{\frac{f\dot{F}_{y,F} - b\dot{F}_{y,R}}{I_{zz}} - \dddot{\psi}_{ref}}_{\lambda(t)} + \underbrace{\frac{\dot{M}_z(t)}{I_{zz}}}_{\tau(t)} \tag{2.28b}$$

Here, M_z is the additional yaw moment induced by the controller and is thus, the control variable. The sub-optimal control law [21] can be then expressed as per equation 2.29.

$$\tau(t) = \frac{\dot{M}_z(t)}{I_{zz}} = -K\text{sign}\Big\{y_1(t) - \frac{1}{2}y_1(t_c)\Big\} \tag{2.29a}$$

$$\dot{M}_z(t) = -I_{zz}K\text{sign}\Big\{y_1(t) - \frac{1}{2}y_1(t_c)\Big\} \tag{2.29b}$$

Here, t_c refers to the time instant at which $\dot{y_1}(t) = 0$, so as to ensure convergence in finite time. Yaw moment rate defined as per equation 2.29 can then be induced by the actuators to achieve the desired boundary condition. Implementation of SMC is discussed later in section 5.1.2.

3
Objective evaluation methods

The objective evaluation methods used throughout the project consists of a set of test manoeuvres for ride comfort and handling. For ride comfort both low frequency and high frequency road excitations were covered. For handling the performance was evaluated in transient and steady state in both the linear and non-linear range.

3.1 Ride comfort

Usually ADAMS Car together with a FTire model is used for ride comfort simulations as it provides reliable results for high frequency road excitations. However this was only possible with passive ARBs due to a lack of of interfaces between the ADAMS model and the simulink model representing the active ARBs. Therefore, only initial simulations with passive ARBs were conducted in ADAMS Car. For the evaluation of the active ARBs influence on ride comfort IPG Carmaker was used together with a Pajecka tyre model. The Pacejka model is a single contact point model in contrast to the multiple contact points used by the FTire model. Hence the reliability of results from high frequency road excitations was expected to be limited due to the lack of the enveloping effect. These simulations are carried out by keeping other ride-control systems (e.g. active suspension and dampers) as inactive.

3.1.1 Ride comfort simulations in ADAMS Car

The ride comfort simulations in ADAMS were conducted using, by Volvo, predefined test scenarios in terms of their ride DNA (RDNA). The vehicle model used were a Volvo XC90. The RDNA consists of multiple scenarios and corresponding measures which aims at evaluating and quantifying a vehicle's ride comfort. Among these measures are for example frequency weighted RMS values of vertical accelerations in different frequency ranges measured when simulating driving on scanned road surfaces. The complete RDNA was evaluated for a XC90 with the original anti-roll bars and the same XC90 model completely without anti-roll bars. By analysing the results key areas which are influenced by the anti-roll bar were identified.

3.1.2 Single sided cosine wave

A single sided cosine wave was used to evaluate the active ARBs effect on the vehicle for road excitations with high amplitude and low frequency. The test was chosen with the purpose of studying the effect of the active ARBs on low frequency roll

motions induced in these kind of road excitations. The procedure used was that the vehicle was travelling on a flat road to let the inbuilt driver model settle to the preset speed. After the flat road the left wheel pair were subject to a cosine wave inducing a roll motion of the vehicle. After the cosine wave the vehicle once again travels on a flat road to enable study of the roll damping.

The profile of the road excitation is shown in Figure 3.1 and the parameters defining the test are presented in Table 3.1. The test was run with three different speeds to alter the frequency of the wheel excitations. The corresponding metrics used for performance evaluation, their definitions and units are presented in Table 3.2.

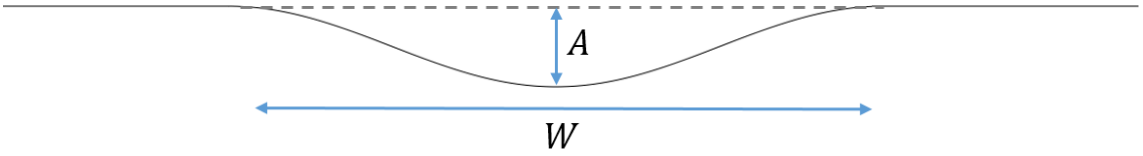

Figure 3.1: Road profile for the cosine wave defined by the wavelength W and the amplitude A.

Table 3.1: Parameters defining the cosine wave road excitation.

Parameter	**Value**
Speed	30, 60 and 90km/h
Amplitude, A	0.1m
Wavelength, W	20m

Table 3.2: Metrics used for the cosine wave road excitations.

Metric	**Unit**	**Comment**
Roll angle φ	deg	-
Roll rate $\dot{\varphi}$	deg/s	-
Roll acceleration $\ddot{\varphi}$	deg/s^2	-
Vertical acceleration a_z	m/s^2	Of vehicle body

3.1.3 Single sided ramp

A single sided excitation in the shape of a ramp followed by a step down to ground level was used to evaluate the high frequency performance of the active ARBs, see Figure 3.2. The procedure used was that the vehicle travelled at a preset speed and after a fixed distance the left wheels were subject to the road excitation. The vehicle continued thereafter drive on a straight road to enable study of the roll damping.

The shape of the road excitations is shown in Figure 3.2 and the parameters defining the profile are presented in Table 3.3. Evaluation of the performance of the active ARBs was conducted using the metrics presented in Table 3.4. Here the focus was put on accelerations rather than roll angle and roll rate due to the short time period of the event, i.e. the effect on roll rate and roll angle is going to be small.

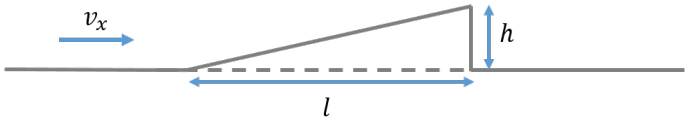

Figure 3.2: Profile of the ramp used in the test. l is the length of the ramp, h is the height and v_x is the speed and corresponding arrow shows the direction of travel.

Table 3.3: Parameters defining the ramp road excitation.

Parameter	**Value**
Speed, v_x	$30km/h$
Height, h	$0.03m$
Length , l	$0.3m$

Table 3.4: Metrics used for the cosine wave road excitations.

Metric	**Unit**	**Comment**
Roll acceleration $\ddot{\varphi}$	$[deg/s^2]$	-
Vertical acceleration a_z	$[m/s^2]$	Of vehicle body and wheels

3.2 Handling

The performance evaluation for the active ARBs in terms of handling was conducted through four manoeuvres. The manoeuvres were chosen to cover all dimensions of the handling of a vehicle, steady state and transient manoeuvres in both the linear and the non-linear range. As the evaluation of active ARBs is to be done independent of other active systems, stability systems like ESC, ABS, traction control etc. were kept inactive during these manoeuvres. Table 3.5 visualises the chosen manoeuvres in relation the the two dimensions. Simulations of these manoeuvres were conducted in IPG Carmaker using an existing model of the XC90 running in parallel with a Simulink model representing the active ARBs.

Table 3.5: Two dimensions of handling performance evaluation and the chosen manoeuvre for each combination.

	Steady state	**Transient**
Linear	Constant radius	Frequency response
Non-linear	Constant radius	Sine with dwell

3.2.1 Constant radius cornering

The steady state cornering test performed was conducted in accordance with the constant radius manoeuvre in ISO 4138:2012 [22]. There exists two variants of this test, one were several discrete speed steps are used and one were the speed of the vehicle is continuously increased slowly until the limit of the vehicle is reached. Here the latter alternative was chosen. The parameters defining the manoeuvre was chosen according to the guidelines in the ISO standard. The exact parameters used are presented in Table 3.6.

Table 3.6: Parameters defining the constant radius manoeuvre according to ISO 4138:2012 [22].

Parameter	**Value**
Radius	100m
Maximum allowed deviation from path	$\pm$0.5m
Maximum allowed increase of a_y	0.2m/s^2/s

Analysis of the vehicle performance in the constant radius manoeuvre was conducted by comparing a number of metrics. In ISO 4138:2012 a set of metrics are suggested but only some of these were considered to be necessary for evaluating the function of the active ARBs. The selected metrics, their definitions and units are presented in Table 3.7.

Table 3.7: Selections of metrics from ISO 4138:2012 used for performance evaluation of the constant radius cornering manoeuvre.

Metric	**Definition**	**Unit**	**Comment**
Roll angle gradient	φ/a_y	deg/m/s^2	-
Understeer coefficient	K_{us}	rad/m/s^2	-

3.2.2 Frequency response

A frequency response test was performed in accordance with the continuous sinusoidal test specified in ISO 7401:2011 [23]. The procedure was that the vehicle drives in a straight line at a set velocity and then a continuous sinusoidal steering wheel angle with increasing frequency was applied while keeping constant throttle input. The parameters specifying the manoeuvre are stated in Table 3.8. Performance evaluation was conducted using a combination of a metric presented in ISO 7401:2011 [23] and one additional metric that was thought to be of importance. The chosen metrics are stated in 3.9.

Table 3.8: Parameters defining the continuous sinusoidal manoeuvre according to ISO 7401:2011 [23].

Parameter	**Value**
Speed	100km/h
Frequency range	$0.1 - 10$Hz
Lateral acceleration a_y	4m/s^2

Table 3.9: Selections of metrics from ISO 7401:2011 used for performance evaluation [23].

Metric	**Definition**	**Unit**	**Comment**
Yaw rate gain	$\dot{\psi}/\delta_{SWA}$	deg/s/deg	In frequency domain
Roll angle gain	φ/a_y	deg/m/s^2	In frequency domain Not included in ISO 7401

3.2.3 Sine with dwell

NHTSA's study on vehicle handling and ESC systems [24] evaluates different manoeuvres for their ability to provide a good assessment of vehicle's handling (and the ESC system's) potential. Several manoeuvres like constant radius circle, slowly increasing steer, sine steer, sine with dwell etc. were evaluated. Sine with dwell was found to generate sufficient yaw and lateral displacement with relatively low steering angles. Thus, the test can be concluded to be ideal for evaluating the vehicle's lateral stability and to best reflect the effect of stiffness distribution between front and rear axle.

The nominal steering wheel angle for the manoeuvre is estimated by performing the slowly increasing steer test and recording the steering wheel input at which 0.3g of lateral acceleration is achieved. Parameters for NHTSA's sine with dwell manoeuvre are listed in Table 3.10.

Table 3.10: Parameters for NHTSA sine with dwell manoeuvre [25].

Parameter	**Value**
Frequency	0.7 Hz
Entrance Speed	50 mph
Dwell time	0.5 seconds
Nominal SWA	$1.5 \cdot$ SWA at 0.3 g
SWA increment	$0.5 \cdot$ SWA at 0.3 g
Maximum SWA	$6.5 \cdot$ SWA at 0.3 g or 270 $\circ$

Few metrics are also analysed in [24] and are found to correctly quantify a vehicle's responsiveness and handling characteristics. In addition to yaw behaviour, it is proposed to analyse these metrics for vehicle's roll as well. This analysis would help in studying the trade-off between the roll and handling performance in the manoeuvre. The metrics used are listed in Table 3.11.

Table 3.11: Metrics for sine with dwell manoeuvre [25].

Metric	**Comment**	**Compliance Range**
Yaw rate ratio I	1 second after COS	<35%
Roll angle ratio I	1 second after COS	
Yaw rate ratio II	1.75 seconds after COS	<20%
Roll angle ratio II	1.75 second after COS	
Lateral displacement	1.07 seconds after BOS	>1.83m

4

Simulations with passive anti-roll bars

Simulations with passive ARBs are conducted to study the effect of the total ARB stiffness and the stiffness distribution on the vehicle behaviour in terms of ride comfort and handling. For the manoeuvres where normalized results are presented, the non-normalized results are found in Appendix B.1.

4.1 Ride comfort

A set of ride comfort simulations are conducted to investigate the impact of ARBs on ride comfort. This with the aim to verify the theory and to establish a starting point for development of the control strategy.

4.1.1 Ride comfort simulations in ADAMS Car

Simulation results from ride comfort evaluations in ADAMS Car shows that the ARBs influences both primary and secondary ride comfort.

Primary ride is primarily influenced in terms of the roll motion of the vehicle. The most significant influence from the ARBs is more specifically seen in a metric called head toss index. Head toss index are supposed to quantify the head toss the driver is subject to. This metric reduces by 6% when the ARBs are removed compare to the same vehicle with ARBs. It is also seen that removal of the ARBs are not necessary to produce a reduction in the head toss index, a reduction of the stiffness is enough.

Secondary ride is primarily influenced in terms of the vertical vibrations in the driver seat rail. In the simulations removal of both ARBs shows to decrease the frequency weighted RMS values of vertical vibrations in the driver seat rail for all simulated frequencies, 3-100 Hz. It is also observed that the most significant reduction is found in the 3-7Hz band where the weighted RMS values are reduced with 13%. The reduction decreases for higher frequencies but due to the frequency weighting, where the lower frequencies are more important, the corresponding values for the interval 3-50Hz is a reduction with close to 7%. The corresponding power spectral density (PSD) of the RMS values is plotted in Figure 4.1 which clearly shows that the largest reduction is found for frequencies between 3-7Hz. As for the head toss index, a reduction in the RMS values of the vertical accelerations are also seen when reducing the ARB stiffness, i.e. removal of the ARBs are not necessary.

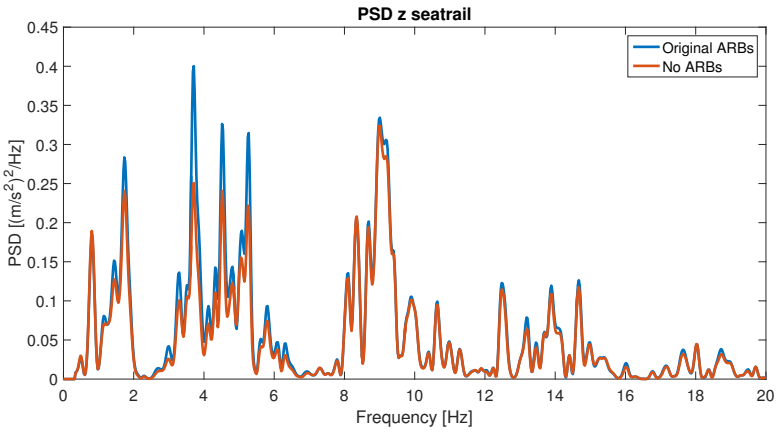

Figure 4.1: PSD of weighted RMS values of vertical vibrations in the seat rail for a vehicle with and without ARBs.

4.1.2 Single sided cosine wave

Figure 4.2a and 4.2b shows the roll angle respectively roll rate as a function of time for a vehicle with and without ARBs travelling in 60km/h while subject to a single sided cosine wave. It is seen that the amplitude of both the negative and positive peaks in roll angle are slightly increased and shifted in time when the ARBs are removed. Furthermore, the same behaviour is consequently observed for the roll rate. It is also seen that both the vehicle with and without ARBs creates a roll overshoot, i.e. when the vehicle exits the dip it overcompensates and rolls right before the roll motion dampens out. The same observations are also made for the two other test speeds 30km/h and 90km/h although with decreased magnitude for the test in 30km/h, see Figures A.2 to A.4 in appendix A. Furthermore, the removal of the ARBs is observed to have no impact on the vertical accelerations for the test speeds 30 and 60km/h while a small increase is seen for the highest test speed 90km/h, see Figures A.2 to A.4 in Appendix A.

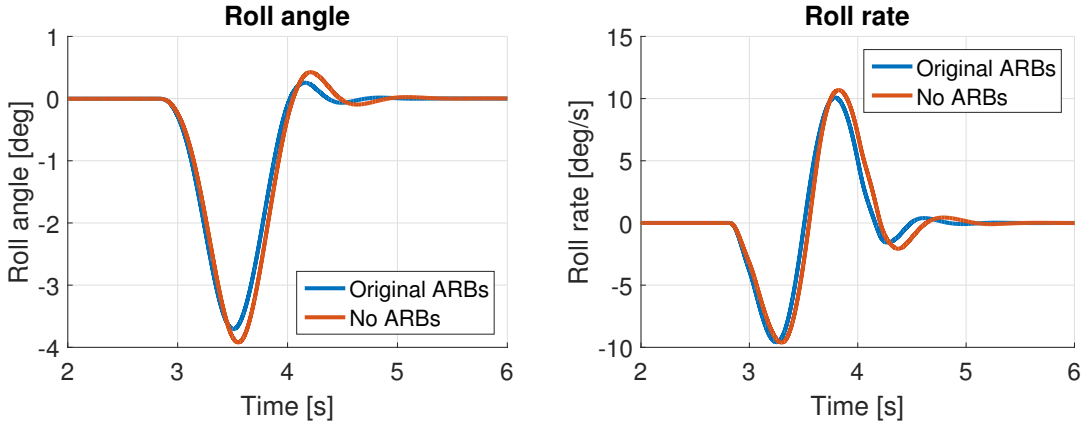

(a) Roll angle **(b)** Roll rate

Figure 4.2: Roll angle (a) and roll rate (b) as a function of time for a single sided cosine wave with a test speed of 60kmh/h.

Further simulations shows that removing only the front or rear ARB does not alter the behaviour of the vehicle substantially. Amplitudes of roll angle and roll rate are in the range between those of a vehicle with and without ARBs as expected, see Figure A.5 in appendix A. Similarly as when both ARBs were removed a slight time shift is seen primarily when removing the front ARB. It is seen that removing the front ARB delays the response from the vehicle, see Figure A.5 in Appendix A.

4.1.3 Single sided ramp

Figure 4.3a shows the roll acceleration as a function of time for a single sided ramp test. It shows that removal of both ARBs reduces the magnitudes of the three largest roll acceleration peaks while the magnitude of the smaller peaks are increased slightly which indicates slightly decreased damping. Figure 4.3b shows simulations results from the same test as previously but with the front respectively rear ARB removed. Comparison of Figure 4.3a and 4.3b shows that the reduction of the magnitude of the first and second roll acceleration peak is solely due to the removal of the front ARB. The same is seen for the rear ARB which is solely responsible for the roll acceleration reduction of the third roll acceleration peak.

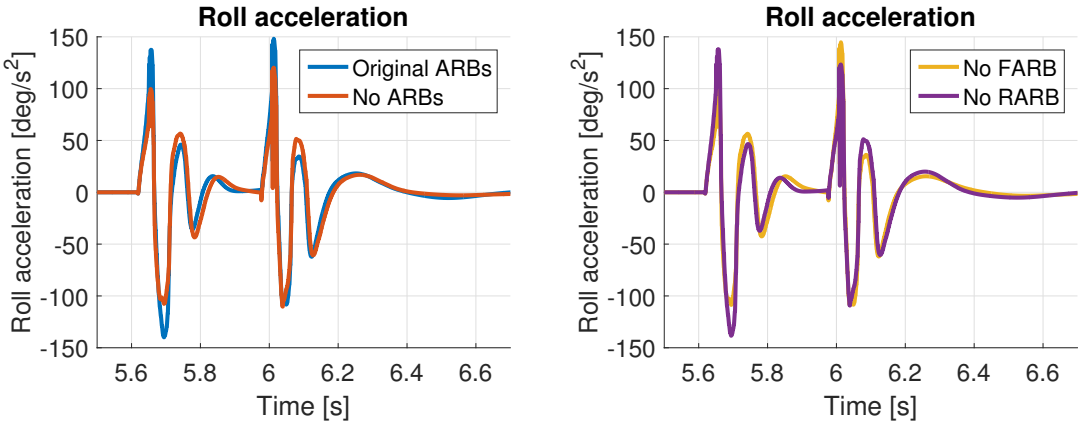

(a) Original ARBs and no ARBs **(b)** No front ARB and no rear ARB

Figure 4.3: Roll acceleration as a function of time for a vehicle with and without ARBs (a) and the same vehicle without front respectively rear ARB (b) for a single sided ramp test.

Figure 4.4 shows the global vertical acceleration of all four wheels for the same single sided ramp test as above. Here it is seen that the copying effect is, as expected from theory, removed with the removal of the respective axles ARBs. When the left wheels hits the ramp the right wheels follows the left wheel when the ARB is present but with it disconnected this phenomenon is removed. However, it can be seen that the right wheel is subject to some small accelerations with the ARBs disconnected which is due to the roll motion of the vehicle which makes the springs and damper push the right wheel down into the ground.

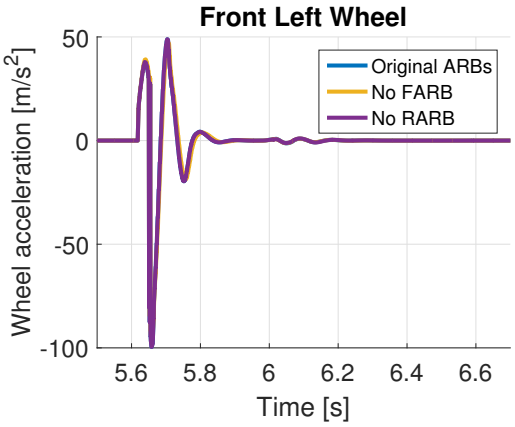

(a) Front left wheel

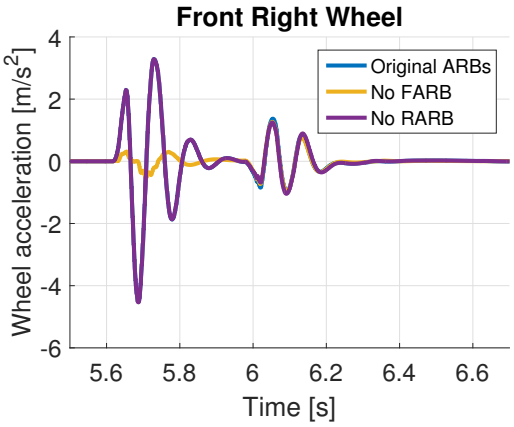

(b) Front right wheel

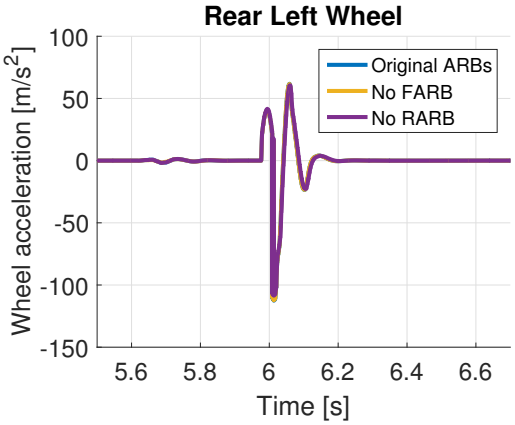

(c) Rear left wheel

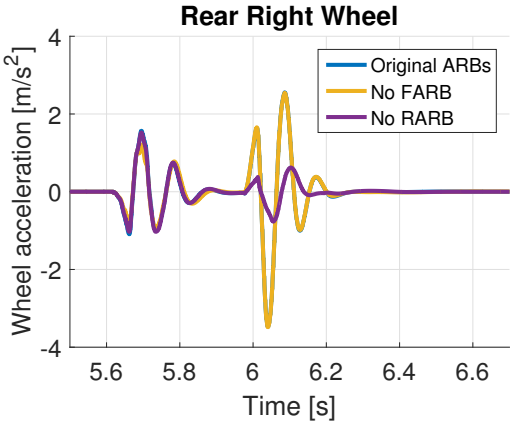

(d) Rear right wheel

Figure 4.4: Wheel acceleration for all four wheels as a function of time for a vehicle with ARBs, without front ARB and without rear ARB for a single sided wave with a test speed of 60kmh/h.

4.2 Handling

A set of simulations are conducted to establish how the passive ARBs influences vehicle handling and in order to verify the theoretical findings. Furthermore these simulations establish the reference for performance evaluation of the active ARBs.

4.2.1 Constant radius cornering

Figure 4.5 shows the roll behaviour of a vehicle with and without ARBs. It can be seen that the roll gradient of the passive vehicle is constant for the studied range of lateral accelerations and removing the ARBs results in a higher roll gradient. This as the vehicle roll stiffness is reduced and only consists of the contributions from the springs and dampers.

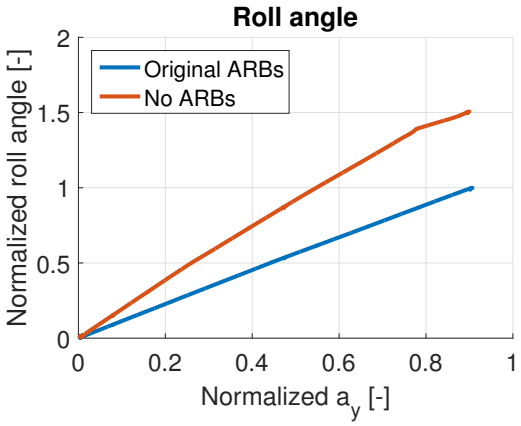

Figure 4.5: Normalised roll angle as function of normalised lateral acceleration for a vehicle with and without ARBs.

As discussed in section 2.3, the effect of ARBs on handling characteristics is dependent on the stiffness distribution between the front and rear axle. Handling behaviour of the car is quantified using the understeer coefficient, K_{us} values. In order to identify the maximum possible effect ARBs can have on handling, extreme cases are required to be simulated by using only one ARB at a time. Figure 4.6 compares the handling characteristics for these cases with the vehicle having default distribution.

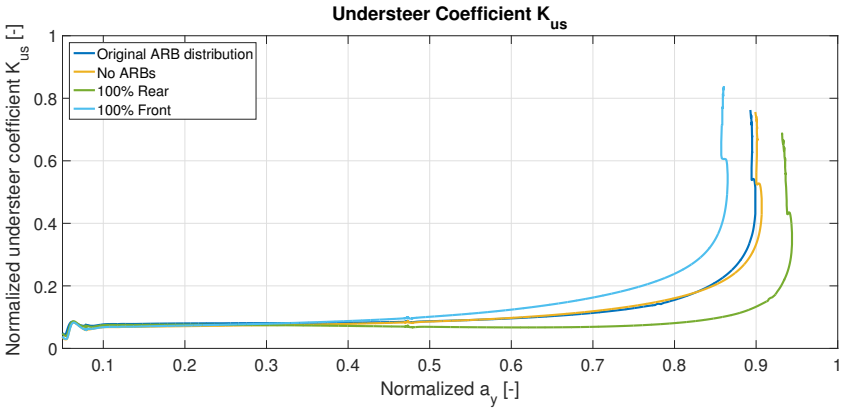

Figure 4.6: Handling characteristics for different stiffness distribution

It is observed from Figure 4.6 that increasing the stiffness at the rear axle reduces the understeering behaviour of the vehicle. This is due to the increase in load transfer and the subsequent loss in cornering stiffness on the rear axle, allowing it to turn faster and requiring less steering input. This change also allows the vehicle to achieve higher values of lateral acceleration. The inverse happens when the stiffness is increased on front axle as the front loses cornering stiffness more easily, requiring an even larger steering input for an identical manoeuvre. It can also be noted that handling characteristics with passive ARB is quite similar to the vehicle without any ARB. This implies that stiffness distribution provided by the ARB on front and rear axle is not very different to the stiffness distribution of the suspension setup.

4.2.2 Frequency response

Figure 4.7 shows the results, in terms of normalized roll angle gain respectively phase angle over frequency, for frequency response simulations for a vehicle with ARBs, without ARBs, without front ARB and without rear ARB. This is to study how the ARB stiffness influences the vehicle roll behaviour. The simulations are conducted according to the test described in section 3.2.2. All results are normalized with the original vehicles steady state roll angle gain.

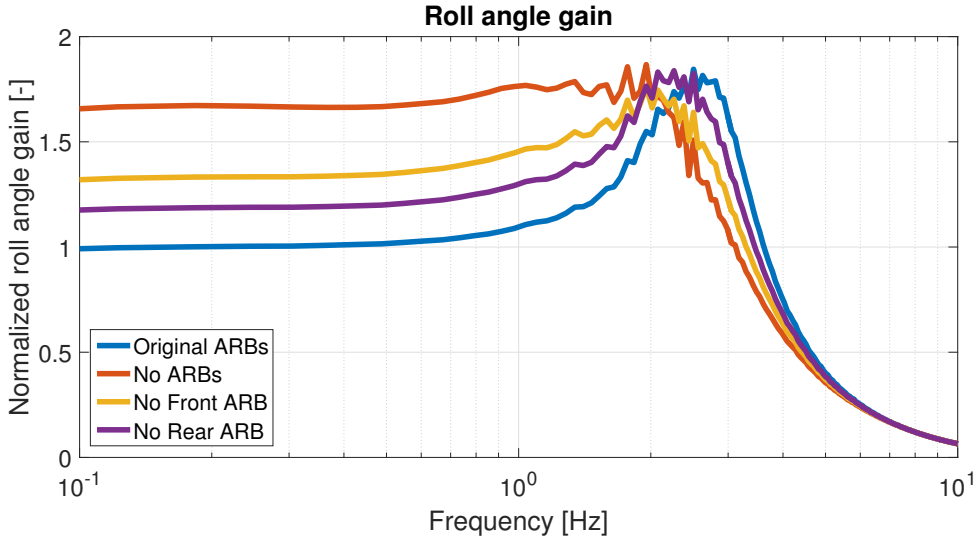

(a) Roll angle gain

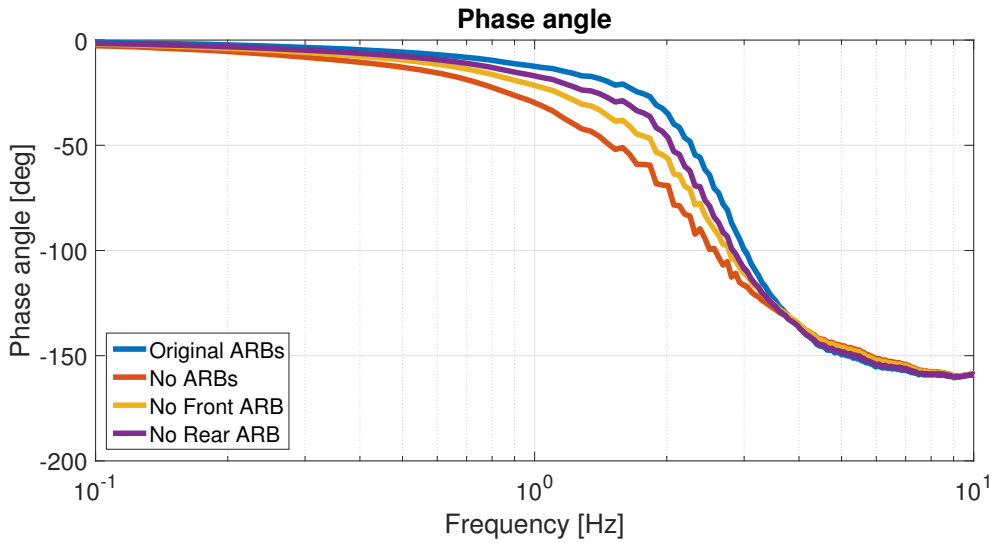

(b) Phase angle

Figure 4.7: Normalized roll angle gain (a) and phase angle (b) for a vehicle with the original, without ARBs, without front ARB and without rear ARB obtained from frequency response simulations.

The simulation results confirm the findings from theory in section 2.2.1 that lowered roll stiffness increases the roll angle gain, shifts the eigenfrequency to a lower frequency and increases the damping ratio. The four different simulations show as expected that the original vehicle has highest roll stiffness followed by the vehicle without rear ARB. Furthermore the vehicle with the lowest stiffness is the vehicle without ARBs followed by the vehicle without front ARB. The same hierarchy is seen for the roll damping, the vehicle without ARBs are close to critically damped, i.e. almost no roll overshoot compared to its steady state value is seen. Worth noting is also that the increased roll damping as expected increases the phase angle in Figure 4.7b, i.e. the time delay between the lateral acceleration peak and the peak in roll angle is increased.

Lastly a coherence analysis of the results shows a coherence of above 98% for all simulations in the studied frequency range. Hence the validity of the results are considered to be high.

The effect of the ARBs on the yaw behaviour during a frequency response manoeuvre for the same vehicle setups as shown in Figure 4.8. The results shows that in steady state the yaw rate gain, see Figure 4.8a is reduced compared to the original vehicle for all ARB combinations. This shows that reducing the roll stiffness in general reduces the yaw rate gain. One reason for this could be the vehicles roll understeer behaviour, i.e. that vehicle roll due to the suspension geometry results in kinematic toe angle changes which results in more understeer and hence lower yaw rate gain. However this needs further investigations to be able to conclude that this is the actual cause. Furthermore, no effect of the roll stiffness distribution is seen on the yaw rate gain in steady state. This is thought to be due to the low lateral accelerations and hence the tyres work in the linear range of the cornering stiffness. Around the yaw rate's eigenfrequency the opposite behaviour is seen, i.e. that a higher yaw rate gain is achieved with lower roll stiffness and higher roll damping. Furthermore it is seen that the yaw rate eigenfrequency is unaltered as a function of the change in roll stiffness.

Lastly, the coherence between the yaw rate signal and the steering wheel angle signal for all four simulations were also good, above 99% for the entire studied frequency range.

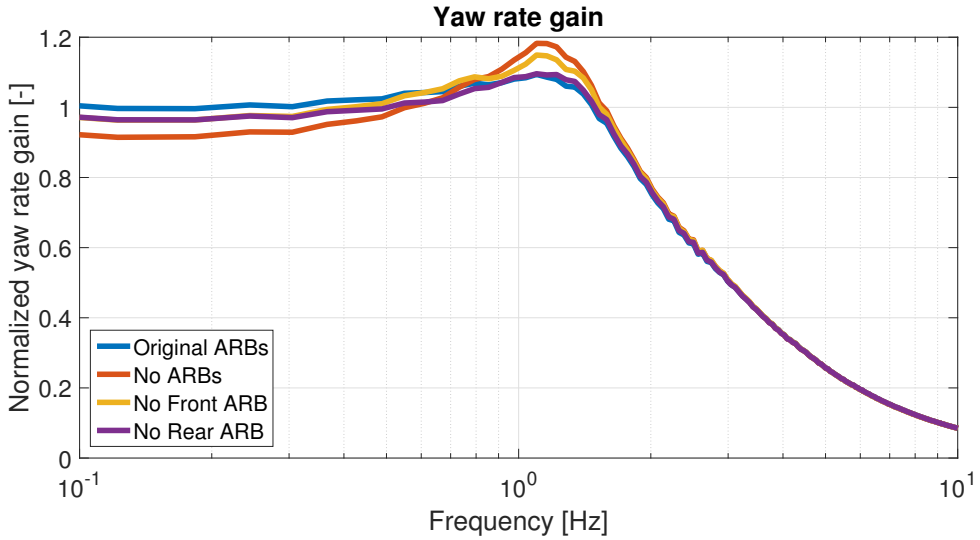

(a) Yaw rate gain

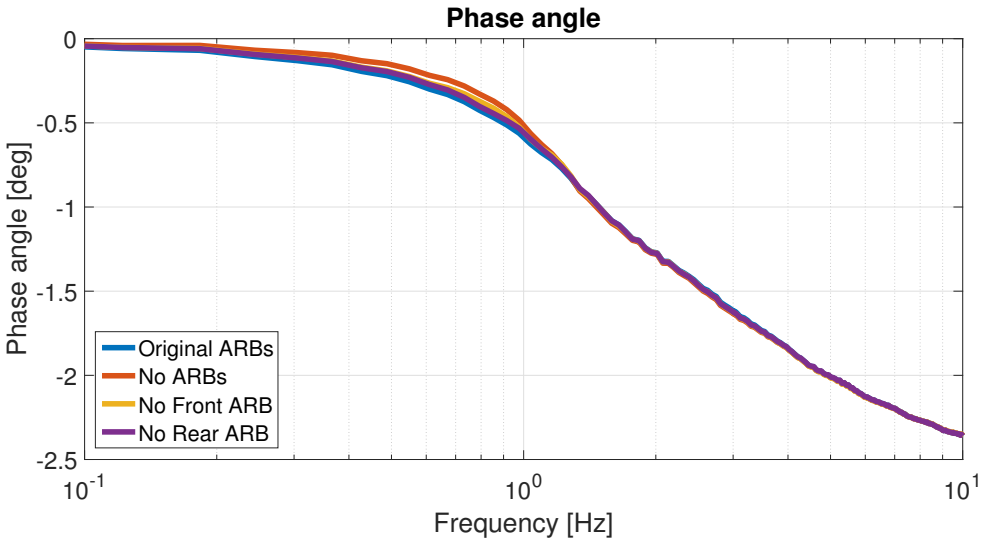

(b) Phase angle

Figure 4.8: Normalized yaw rate gain (a) and phase angle (b) for a vehicle with the original, without ARBs, without front ARB and without rear ARB obtained from frequency response simulations.

4.2.3 Sine with dwell

In order to study the effect of ARB on handling in non-linear transient conditions, sine with dwell tests are carried out with and without ARB. By increasing the SWA in steps, the maximum steering angle is identified for which metrics are within the standard's specified limits. For metric data, refer Appendix B.3. Figures 4.9 and Figure 4.10 show the effect of ARB on vehicle's yaw and roll behaviour respectively.

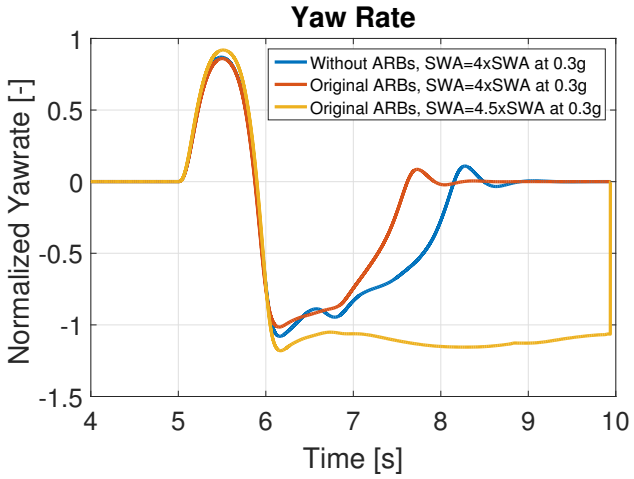

Figure 4.9: Normalised yaw behaviour for a vehicle with and without ARBs.

It is observed from Figure 4.9 that for a steering input of 4 times SWA at 0.3g, yaw damping is substantially improved with use of ARBs. The next test is performed with a higher steering angle, i.e. 4.5 times SWA at 0.3g. In this test, passive ARBs are not able to provide sufficient lateral stability and the vehicle undergoes excessive yaw motion. Similar observations are made with roll performance of the vehicle, as shown in Figure 4.10.

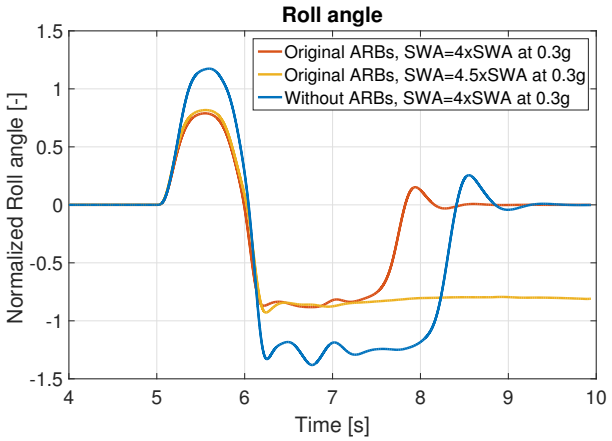

Figure 4.10: Normalised roll behaviour for a vehicle with and without ARBs.

From the results illustrated in Figure 4.10, it can be seen that the vehicle with ARBs rolls more compared to the vehicle without ARBs. When using ARBs, a direct dependency of roll angle behaviour over yaw rate behaviour is also observed.

5
Control strategy

The control strategy developed for active ARBs can be interpreted as a combination of two distinct sub-level controllers, the stiffness controller and the distribution controller. The stiffness controller is responsible for controlling the roll angle of the vehicle and maintaining ride comfort. The task of the distribution controller is to determine the appropriate load transfer distribution between the front and rear axle. Figure 5.1 shows an overview of the developed control strategy with inputs and outputs specified. Some of the results presented in this chapter are normalized. For corresponding non-normalized results see Appendix B.2.

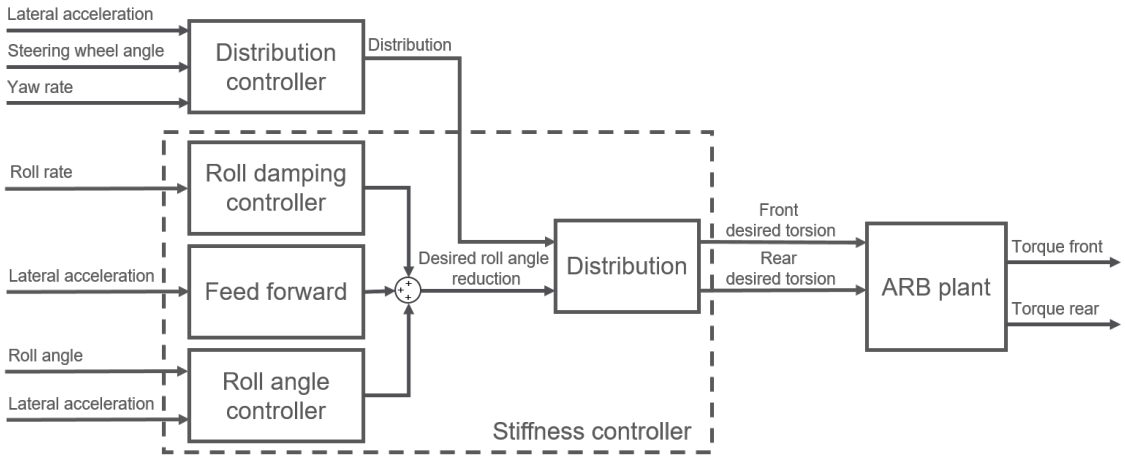

Figure 5.1: Overview of the developed controller.

5.1 Distribution controller

Distribution controller monitors the yaw dynamics of the vehicle and controls the load transfer distribution between the front and rear axle in order to achieve the desired handling characteristics. An overview of the distribution controller is shown in Figure 5.2.

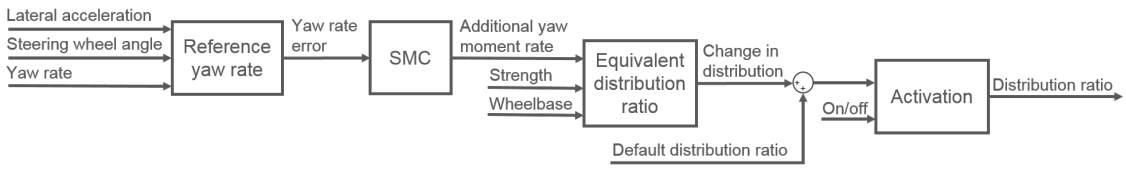

Figure 5.2: Overview of distribution controller

The reference yaw rate block calculates the yaw rate error which is used by the SMC to estimate an additional yaw moment rate. The yaw moment rate is converted into an equivalent change in lateral force and subsequently, to the required change in load transfer distribution that would create the corresponding rate of yaw moment. An activation logic determines if the distribution control system should be active or whether the vehicle should operate on the default distribution ratio. The ratio is between the load transfer that occurs on the front axle and the total load transfer on front and rear axle. The output of the distribution controller does not take the geometries of the front and rear suspension into consideration. Apart from the front and rear ARB stiffness, factors like arm length, motion ratio and track width can also influence the effective roll moment distribution and thus, should be accounted for in the control model.

5.1.1 Reference yaw rate

As discussed in section 2.3.2, equations for yaw dynamics are based on a bicycle model and the expression for vehicle's yaw rate in steady state condition is given by equation 2.18. Figure 5.3 illustrated the implementation of the bicycle model in the controller for generation of reference yaw-rate.

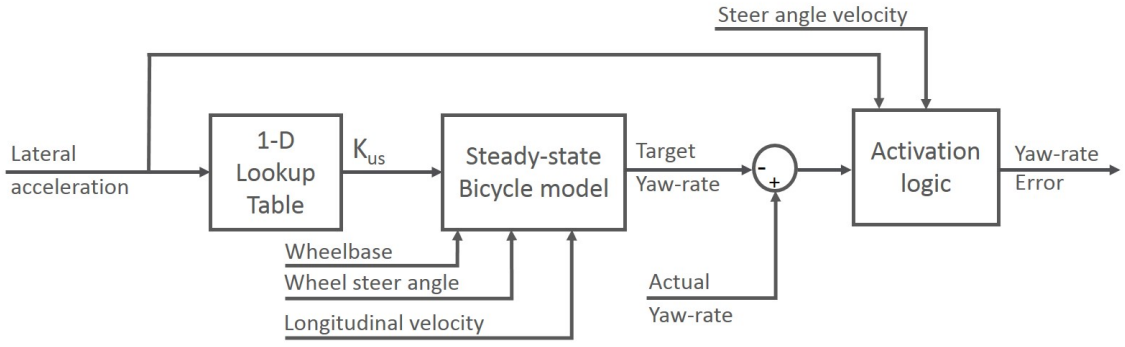

Figure 5.3: Logic for reference yaw-rate generation

As can be seen in Figure 5.3, determination of reference yaw rate requires specification of the understeer coefficient. As the requirements for understeer behaviour are subjective and vary depending on vehicle model and OEMs, a hypothetical understeer behaviour is fed to the controller in form of a lateral acceleration based 1-D lookup table, refer Figure A.1 in Appendix A. The reference understeer coefficient takes into account the handling potential of active ARBs, as discussed in Chapter 6. An activation algorithm is also required to be implemented such that the distribution controller remains deactivated during straight line driving. The controller is deactivated whenever both lateral acceleration and steering angle velocity fall below a certain reference value.

5.1.2 Sliding mode control

The control law for SMC is expressed using equation 2.29 for application in yaw dynamics control. But, there are certain limitations in the direct application of the control equation.

Firstly, as the ARB plant is designed to operate in defined time steps and the control law requires the detection of the condition $\dot{y_1}(t) = 0$, it is not possible to simply implement this functionality using the 'Compare to Zero' block in Simulink. Instead of monitoring the values of $\dot{y_1}(t)$, only the sign of two consecutive values are observed. The condition $\dot{y_1}(t_1) \cdot \dot{y_1}(t_1 + \Delta t) < 0$ for these consecutive instances is checked with help of 'Unit Delay' block. The original condition, $\dot{y_1}(t) = 0$ is fulfilled in the intermediate time interval. The error at this condition gets saved using the 'Unit Delay' block as well.

Secondly, it was noted that implementation of sign function results in aggressive switching in the controller output. Sign function is substituted with the function in equation 5.1, to smoothen the controller response.

$$\text{sign}(y_1) \approx \frac{y_1}{e + \mid y_1 \mid} \tag{5.1}$$

Value of e, along with the constant K from equation 2.29 can be tuned for desired stability and behaviour. Figure 5.4 compares the output of the distribution controller using sign function and the function defined in 5.1 for a typical sine with dwell manoeuvre.

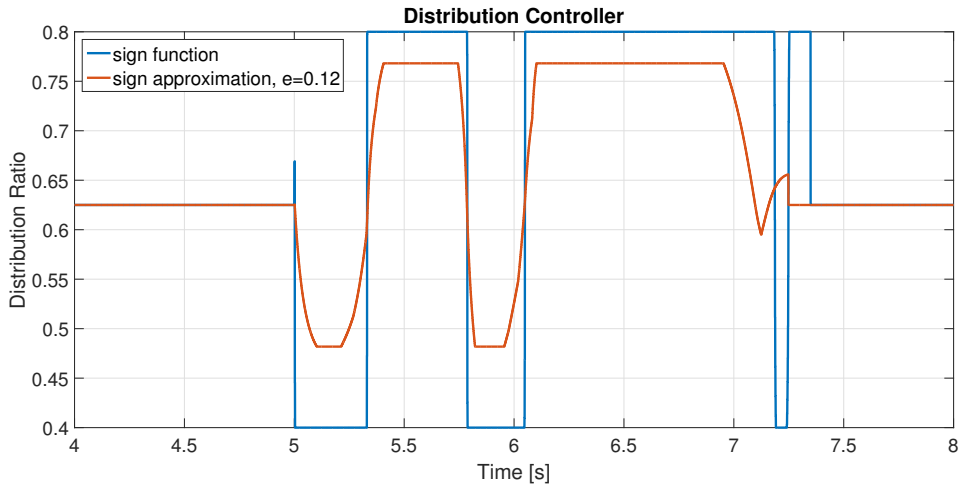

Figure 5.4: Stability of distribution controller

As seen from Figure 5.4, the function in equation 5.1 adds robustness to the controller. Figure 5.5 illustrates the implementation the sliding mode control strategy within the distribution controller subsystem.

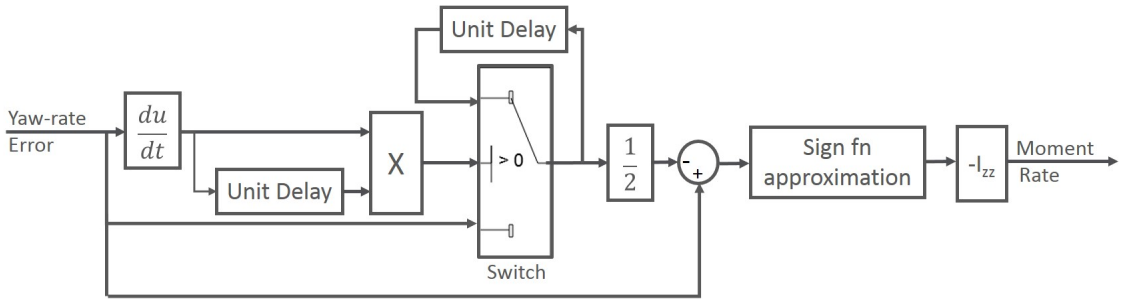

Figure 5.5: Control logic for Sliding Mode Control

5.2 Stiffness controller

The stiffness controller controls the roll behaviour of the vehicle due to both lateral accelerations and road excitations. The execution chosen is a controller built up by three control segments, see Figure 5.1. The first is a ride comfort oriented controller whose primary focus is to increase the roll damping. Furthermore, two additional controllers are used to control the roll angle of the vehicle during cornering. These two are a feed forward control which predicts the required roll angle reduction and corresponding control signals and an I-controller for roll angle which aims at eliminating the remaining error that might occur due to inaccurate predictions by the feed forward.

The outputs from these three control segments are a total desired roll angle reduction. The total desired roll angle reduction is distributed to the front and rear ARB by a distributor which takes the stiffness of the two ARBs and the track widths front and rear into account. The ratio between the two control signals will therefore always correspond to the desired load transfer distribution independently of the stiffness's of the two ARBs and differences in track width between the front and rear axle.

The control signal sent to the active ARBs are required torsion angles. Hence the desired roll angle reductions are recalculated to torsion angles using the relation presented in equation 2.4. Here the expression for the rear axle is used to calculate the desired torsion on the front axle, this to compensate for the mechanical interfaces between the ARBs and the wheels. This enables to maintain the desired load transfer distribution irrespective of the different mechanical interfaces.

Furthermore the active ARBs are limited in torque output and to ensure that the distribution is maintained a saturation logic is used.

5.2.1 Roll damping controller

The roll damping controller is a PI-controller for roll rate which uses the error between a roll rate reference and the actual, from for example a gyroscope measured, roll rate of the vehicle. Figure 5.6 shows the control scheme for the mentioned controller. The aim with this controller is to increase ride comfort by increasing the roll damping of the vehicle and increase the isolation between road excitations and body roll. The purpose with increasing the roll damping is to eliminate roll angle overshoot seen in section 4.1.2 and create a faster decay of external disturbances seen in section 4.1.3. The roll rate reference is here always set to zero as the controller is aimed to increase ride comfort primarily. Setting the reference to a nonzero roll rate would make the vehicle try to maintain a constant roll rate, i.e. have a continuous roll motion, which is not desired.

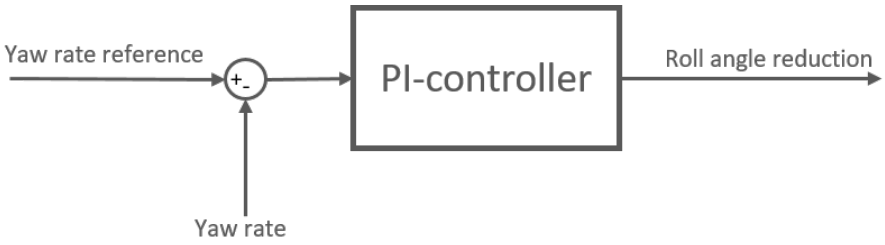

Figure 5.6: Control scheme for the roll damping controller.

The choice of a PI-controller is a key to achieve the above mentioned performance of the system. As seen in the theory presented in section 2.5.2 the P-part of a PID controller based on roll rate increases the roll damping of the vehicle while the I-part increases the roll stiffness of the vehicle. Figure 5.7a and 5.7b shows the implementation of a P- and an I- controller for roll rate in a single sided cosine wave with a test speed of 60km/h.

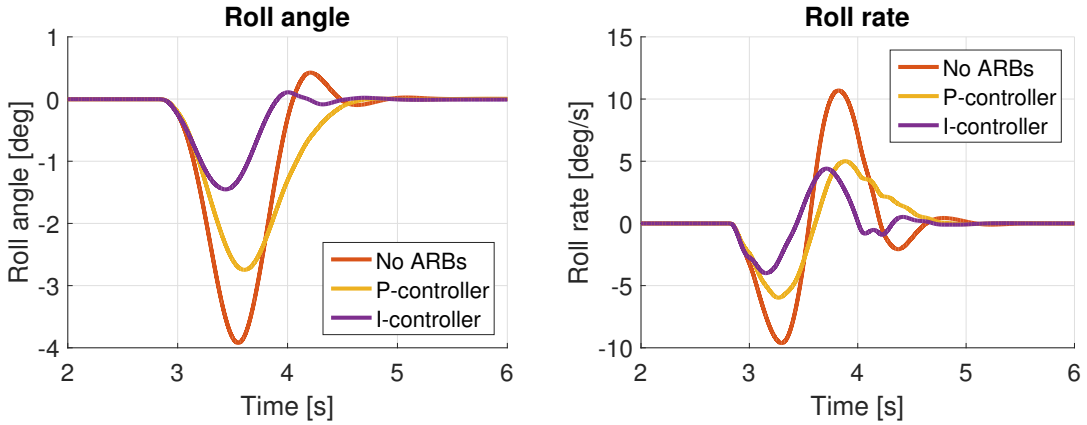

(a) Roll angle **(b)** Roll rate

Figure 5.7: Impact of a P- and an I-controller for roll rate on a vehicle in terms of roll angle (a) and roll rate (b). The test is a single sided cosine wave with a test speed of 60kmh/h.

The results from Figure 5.7a and 5.7b verifies the theoretical findings as the P-controller increases the damping of the system and as desired removes the roll angle overshoot. It can also be seen that the increased damping also reduces the peak roll angle. The I-controller is seen to increase the stiffness of the system as the peak roll angle of the system is heavily reduced. Furthermore it can also be seen that the damping of the roll motion is decreased with the increased stiffness as expected from the theoretical findings.

From these results it is concluded that by altering the tuning of the P- and I-parameter of the PI controller the characteristics of the vehicle might be altered. A higher P-value increases the damping while a higher I-value increases the roll stiffness. These two parameters needs to be tuned in parallel as higher I-value increases the stiffness which requires a higher P-value to obtain the same damping of the system. A risk identified is that a to high P-value makes the vehicle over damped, i.e. the roll angle is reduced but maintained for a longer time. This is expected to be a undesired behaviour from the drivers perspective as it might induce a feel of lack of connection with the vehicle.

5.2.2 Feed forward

The control strategy for roll reduction during cornering is based on an approach where the vehicle with passive ARBs is used as a reference. The roll angle desired for the vehicle with active ARBs is expressed as a reference gain G_{ref} times the roll angle for the reference vehicle. This is convenient as the ARBs are implemented on an existing car with passive ARBs and hence the performance of the active ARBs can easily be related to the original vehicle. However, the controller is designed so that any desired roll behaviour as a function of lateral acceleration can be used as the reference roll angle, i.e. the passive vehicle does not have to be used as reference.

To enable quick response of the controller a feed forward control based on lateral acceleration a_y is used. The primary aim with the feed forward control is not be accurate but to give an quick rough estimate of what control signal is needed and thereby reduce the needed work by the other controllers.

The feed forward control calculates the required roll angle reduction based on the lateral acceleration a_y and the transfer function derived in section 2.2.1. The required roll angle reduction $\varphi_{reduction}$ is the difference between the roll angle for a vehicle without ARBs and the desired roll angle, see equation 5.2.

$$\varphi_{reduction} = (H(s)_{NoARBs} - H(s)_{PassiveARBs} G_{ref}) a_y(s) \tag{5.2}$$

Figure 5.8 shows the bode plots for the analytically determined transfer functions, see section 2.2.1, compared to estimated transfer functions. The estimated transfer functions are estimated from simulation results from a frequency response test with a vehicle with and one without ARBs. The coherence for the estimated transfer functions are 98% for the vehicle with ARBs and 95% for the vehicle without ARBs. It can be seen that the estimated transfer functions are accurate in steady state but deviates around the eigenfrequency. As the steady state roll behaviour of the vehicle is determined by the roll stiffness the estimation of the stiffness can be

concluded to be accurate. Furthermore, according to theory the eigenfrequency is determined by the stiffness and the roll inertia. Thus the shift in eigenfrequency between the estimated and analytically determined transfer function can be concluded to be due to a discrepancy in the roll inertia. Furthermore it is also concluded that there is a discrepancy in the roll damping as the discrepancy in roll inertia is not seen to fully remove the discrepancy in the damping behaviour. One reason for this discrepancy in the damping might be that the roll damping is hard to estimate due to the nonlinear behaviour of dampers, i.e. different damper rates for bump and rebound and the damping rates dependency of velocity.

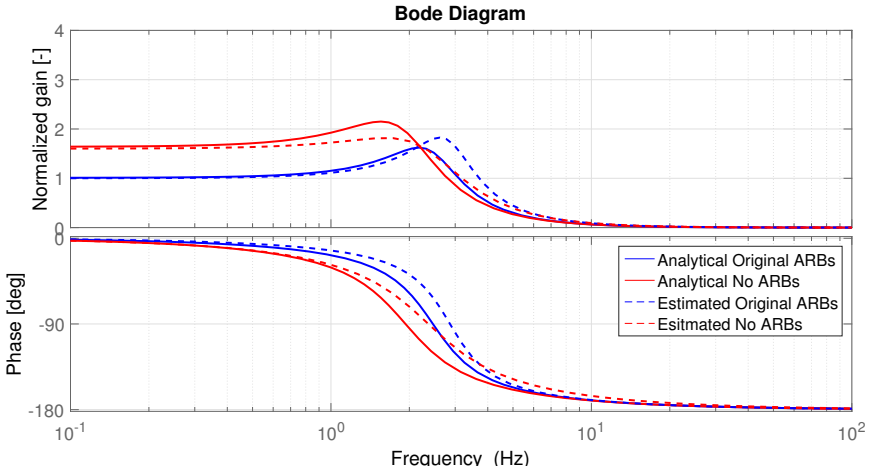

Figure 5.8: Bode plot for the estimated and analytically determined transfer functions from the lateral acceleration a_y to the roll angle φ.

Based on the observed discrepancies between the estimated and analytically determined transfer functions the estimated transfer functions are used in the feed forward controller. The performance of the feed forward control for a constant cornering test is seen in Figure 5.9. Here a reference gain G_{ref} of 1 is used with the purpose of trying to replicate the behaviour of the vehicle with passive ARBs. The simulations shows that the feed forward is able to follow the reference.

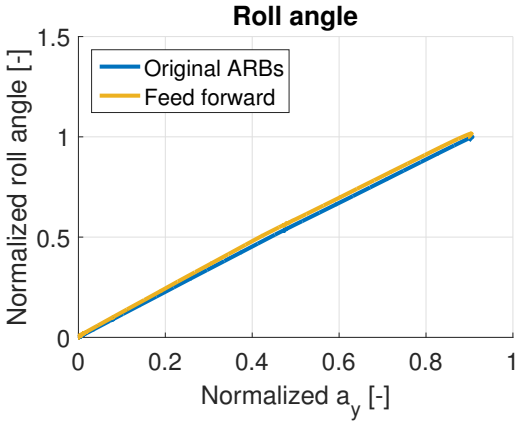

Figure 5.9: Normalised roll angle φ as a function of normalised lateral acceleration a_y for a constant radius cornering test.

One of the biggest benefits with the feed forward control is that it is only dependant on the lateral acceleration of the vehicle. i.e. it will not interfere with ride comfort during driving in low lateral accelerations. Hence the feed forward control can for example be kept active during straight line driving without interfering with the ride comfort of the vehicle.

5.2.3 Roll angle controller

The results from the simulations with the feed forward control showed that its performance was good. However, the feed forward will only work in very specific cases and it is not able to account for eventual disturbances. These could for example be the number of passengers in the vehicle which will influence the vehicle mass and hence alter the behaviour of the vehicle. To be able to compensate for these unknown disturbances a feedback controller is needed.

The roll damping controller described in section 5.2.1 is a feedback controller but will not help in this aspect. This as the roll damping controller always works with trying to eliminate roll rate, i.e. the I-part of the controller will try to maintain zero roll angle. Here a simple but not optimal solution is chosen. An I-controller for roll angle is introduced with the purpose of correcting for the eventual disturbances and for the control signal from the roll damping controllers I-part.

Figure 5.10 shows simulation results from a constant radius cornering test with a vehicle with an extra weight of 200kg. It can be seen that the feed forward is not able to follow the reference which in this simulation is the vehicle with passive ARBs. Furthermore, introducing the roll angle controller and the roll damping controller it is seen that the roll angle deviation is eliminated.

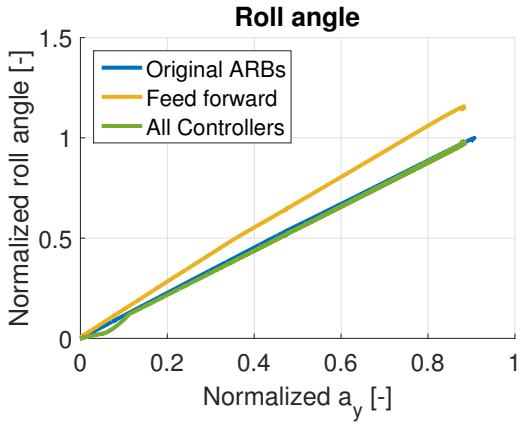

Figure 5.10: Normalised roll angle as a function of normalised lateral acceleration, from a constant radius cornering test for a vehicle with increased mass.

The last part of the roll angle controller is the merger which deactivates the roll angle controller if the lateral acceleration is below a certain threshold. This as the roll angle controller will otherwise conflict with the ride comfort of the vehicle. This as during for example a single sided cosine wave maintaining a certain roll angle is not the objective, hence the roll angle controller will interfere. This merger has a slight side effect on the roll behaviour of the vehicle. In Figure 5.10 it can

be seen that the roll angle is not able to compensate for the error in roll angle for normalized lateral acceleration lower than 0.1. This is due to the inactivated roll angle controller. Inactivating an I-controller might also lead to windup of the integral of the error. For example when driving on a straight road and the vehicle rolls left the integral of the error will build up. As the controller is not active it cannot compensate for this buildup in error until it is activated again. This could give rise to unwanted control signals when the controller is activated the next time. The used solution for this is letting the controller track the control signals from the feed forward and the roll damping controller. Furthermore, similar problems might occur if the active ARBs are not able to maintain a certain roll angle due to limitations in response time or maximum torque. This is solved by feeding back the output from the ARB plant and converting that to a corresponding roll angle reduction and reducing the integral of the error with the difference between the desired roll angle reduction and the actual achieved roll angle reduction. This way windup of the integral is reduced.

5.2.4 Distribution compensation

The moment distribution estimated using the distribution controller in section 5.1 does not take into account the influence of kinematic variables like motion ratio, arm length, track width and difference between torsional stiffness of ARBs at front and rear axle. This section identifies different factors that must be accounted for before a torque request is made to ARB plant, in order to achieve the target moment distribution.

Roll moment at the front and the rear axle is defined as per equation 5.3.

$$M_F = (k_{\varphi,F}.\varphi_F)w_F \tag{5.3a}$$
$$M_R = (k_{\varphi,R}.\varphi_R)w_R \tag{5.3b}$$

A ratio is obtained for roll angle reduction on front and rear axles as per equation 5.4.

$$\frac{\varphi_F}{\varphi_R} = \frac{M_F}{M_R} \cdot \frac{k_{\varphi,R}}{k_{\varphi,F}} \cdot \frac{w_R}{w_F} \tag{5.4}$$

The roll stiffness can be substituted with the torsional stiffness of anti-roll bars as per equation 5.5 to obtain the ratio defined in equation 5.6.

$$k_{\varphi,F} = k_{\gamma,F}.\left(\frac{w_F i_F}{r_F}\right)^2 \tag{5.5a}$$
$$k_{\varphi,R} = k_{\gamma,R}.\left(\frac{w_R i_R}{r_R}\right)^2 \tag{5.5b}$$

$$\frac{\varphi_F}{\varphi_R} \cdot \frac{(\frac{w_F i_F}{r_F})^2}{(\frac{w_R i_R}{r_R})^2} = \frac{M_F}{M_R} \cdot \frac{k_{\gamma,R}}{k_{\gamma,F}} \cdot \frac{w_R}{w_F} = \frac{dist.k_{\gamma,R}.w_R}{(1-dist).k_{\gamma,F}.w_F} \tag{5.6}$$

The ratio in 5.6 can be then used to define the ratio of torsion angles as explained in equation 5.7,

$$\frac{\gamma_F}{\gamma_R} = \frac{\varphi_F}{\varphi_R} \cdot \frac{(\frac{w_F i_F}{r_F})}{(\frac{w_R i_R}{r_R})} = \left(\frac{dist.k_{\gamma,R}.w_R}{(1-dist).k_{\gamma,F}.w_F} \right) \cdot \frac{(\frac{w_R i_R}{r_R})}{(\frac{w_F i_F}{r_F})} \tag{5.7}$$

5.2.5 Saturation

As the specifications of ARB systems can vary, it is required to take the hardware limitation of the active ARBs into consideration when performing simulations. The maximum requested torque can not be allowed to exceed the rated torque of the particular ARB design being evaluated. A control logic is designed that limits the maximum torsion request, see Algorithm 1.

Algorithm 1: Torque saturation

```
front torque = front stiffness * front torsion;
rear torque = rear stiffness * rear torsion;
if abs(front torque) > Torque Limit then
    front torsion = sign(front torque) * Torque Limit / front stiffness;
    if distribution > 0.5 then
        rear torsion = front torsion * ((1-distribution)/distribution);
    else
        rear torsion = front torsion;
    end
else if abs(rear torque) > Torque Limit and distribution < 0.5 then
    rear torsion = sign(rear torque) * Torque Limit / rear stiffness;
    front torsion = rear torsion / ((1-distribution)/distribution);
else
    front torsion = front torsion;
    rear torsion = rear torsion;
end
```

It can be noted in Algorithm 1 that whenever the equivalent torque on an ARB exceeds the limit, torsion gets reduced to the specified limit and the ARB on the other axle follows the saturated ARB as per the distribution. In the case when torque on both ARBs are more than the limit, minimum distribution is limited to 0.5 to provide best possible balance between total roll stiffness and moment distribution. In the default case, when neither of the ARB is at the limit, pre-determined torsion inputs are maintained. The algorithm is seen implemented in Figure 5.11 for a constant radius cornering test.

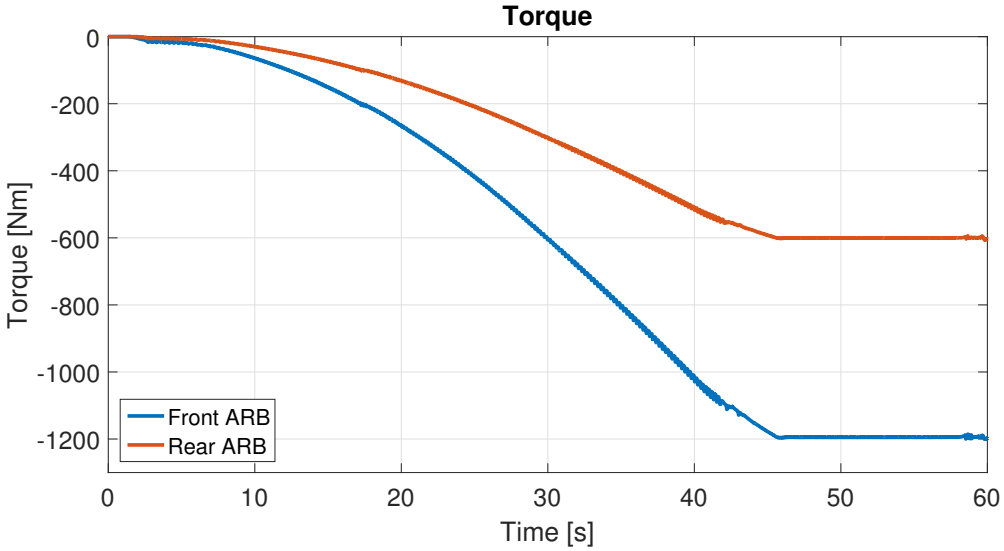

Figure 5.11: Saturation of torque output for constant radius cornering manoeuvre.

Another functionality required to be implemented along with saturation of torque is the treatment of distribution at high lateral acceleration conditions. It is noted that when the vehicle looses grip and starts to slip, the controller tries to induce yaw motion with excessive increase of ARB stiffness on the rear axle. This reaction causes a disproportionate increase in roll stiffness of the vehicle leading to an unexpected decrease in roll angle. The condition is most prominent in steady state manoeuvre, see Figure 5.12.

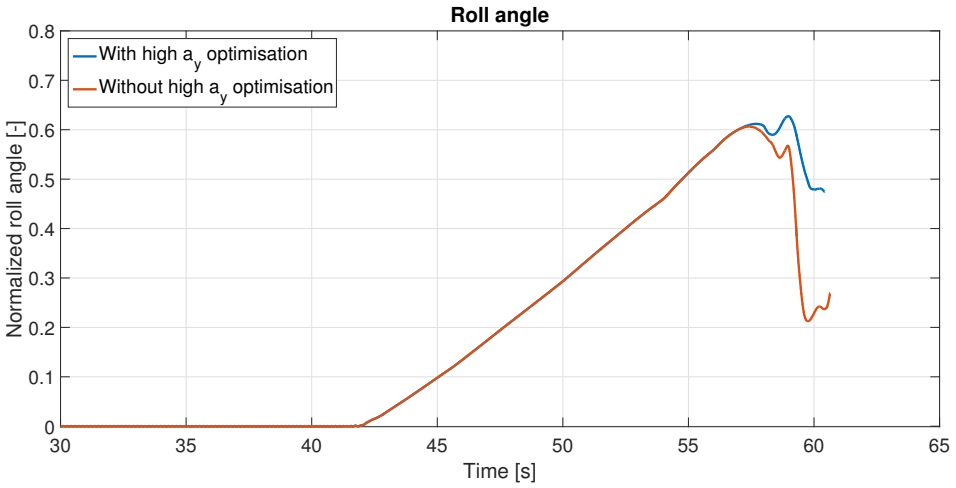

Figure 5.12: Unnatural roll behaviour during high lateral accelerations

The controller is optimised for high lateral accelerations by limiting the distribution ratio during these conditions. Above a specified lateral acceleration value, the distribution ratio is never reduced and thus, total roll stiffness is preserved, as seen in Figure 5.12 and 5.13.

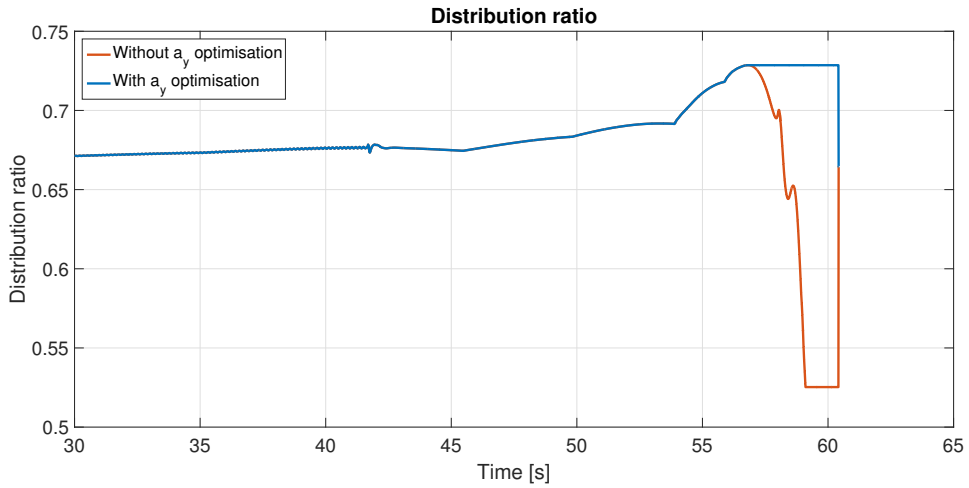

Figure 5.13: Distribution strategy for high lateral accelerations

6
Simulations with active anti-roll bars

This chapter presents the final results from implementing the developed control strategy into the existing vehicle model. Simulation results from both ride comfort simulations and handling simulations are presented. The aim is to show the potential of active ARBs with the chosen control strategy and the extent to which it is affected by the suspension geometry of vehicle. Furthermore, limitations of active ARBs and the current control strategy are also shown and exemplified.

For the non-normalized results from manoeuvres, refer Appendix B.1.

6.1 Ride comfort

Two types of ride comfort simulations are conducted, single sided cosine wave and single sided ramp. The controller performance in these manoeuvres is evaluated and analysed to obtain a understanding of the limitations of the active ARBs and the control strategy.

6.1.1 Single sided cosine wave

Multiple single sided cosine wave tests are simulated to evaluate the performance of the complete controller and showcase how the active ARBs affects the vehicle compared to the original ARBs. Furthermore, the influence of test speed on the combined performance of the controller and active ARBs is investigated.

6.1.1.1 Controller performance

The performance in the single sided cosine wave test is evaluated by running a simulation with a test speed of 60km/h with the complete stiffness controller activated. This means that the roll damping controller, the feed forward and the roll angle controller are all used with a tuning that works for all test cases taken into account in this thesis, both ride comfort test cases and handling test cases. Furthermore, these simulations are conducted with fixed load transfer distribution corresponding to the load transfer distribution of the vehicle with the original ARBs.

Figure 6.1a shows the roll angle as a function of time for a single sided cosine wave test with a test speed of 60km/h. It can be seen that the roll angle is reduced to about -1 degree compared to -3.7 degrees for the vehicle with passive ARBs.

Furthermore, the roll damping is also increased as the roll overshoot seen for the passive vehicle is completely removed.

The roll rate as a function of time for the same simulation can be seen in Figure 6.1b. The results show that the peak roll rates are reduced and that small oscillations in the roll rate signal are induced by the controller.

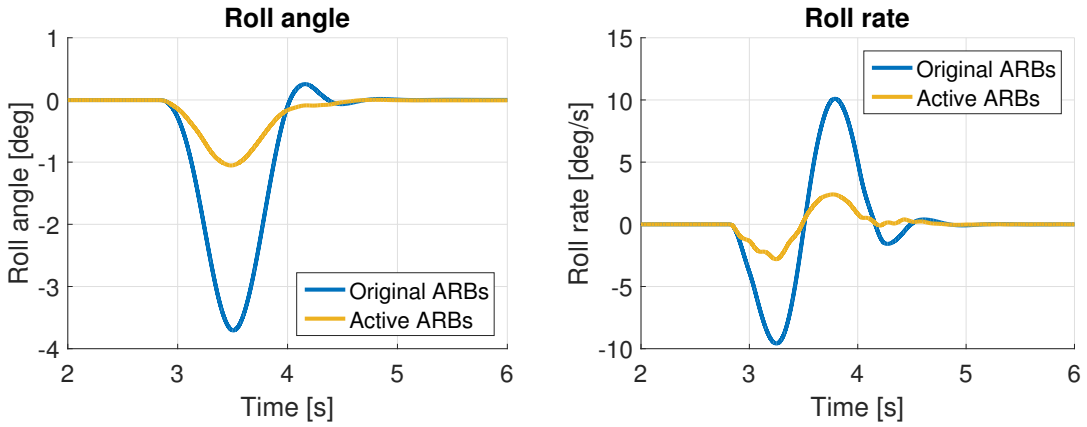

(a) Roll angle **(b)** Roll rate

Figure 6.1: Roll angle (a) and roll rate (b) as a function of time for a single sided cosine wave test with a test speed of 60km/h.

Figure 6.2a shows the roll acceleration from the same simulation as above. Here also the oscillations are visible and it can be concluded that the controller overall reduces the RMS values of the roll acceleration but the frequency composition is shifted towards higher frequencies compared to the vehicle with the original ARBs. Furthermore, the peak vertical acceleration on the vehicle body seen in Figure 6.2b is slightly reduced due to the active ARBs.

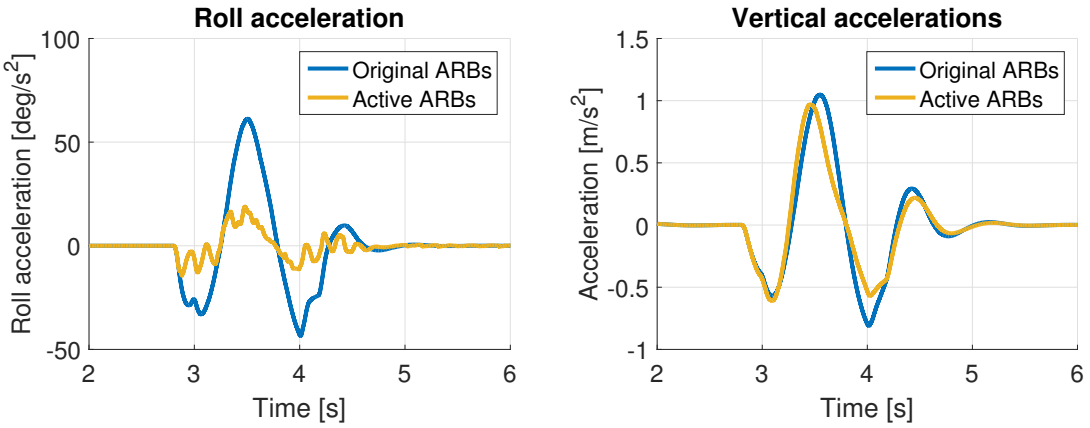

(a) Roll acceleration **(b)** Vertical acceleration

Figure 6.2: Roll acceleration (a) and vertical acceleration (b) as a function of time for a single sided cosine wave test with a test speed of 60km/h.

Figure 6.3 shows how the active ARBs, in terms of wheel forces, are acting to reduce the roll rate and roll angle of the vehicle compared to passive ARBs. It can be seen that the front active ARB initially works in the opposite direction compared to the passive ARB. The active ARB reduces vehicle roll by pushing the left front wheel into the ground and lifting the right front wheel while the passive ARB induces more roll by doing the opposite. On the rear axle, both the passive and active ARB are initially working to reduce the roll motion of the vehicle. After the initial phase the passive ARBs changes direction of the forces applied on the wheels due to the roll angle of the vehicle. Whereas, the active ARB maintains the direction of the forces for a longer period of time and at the end of the dip, changes direction of the forces to counteract the roll overshoot.

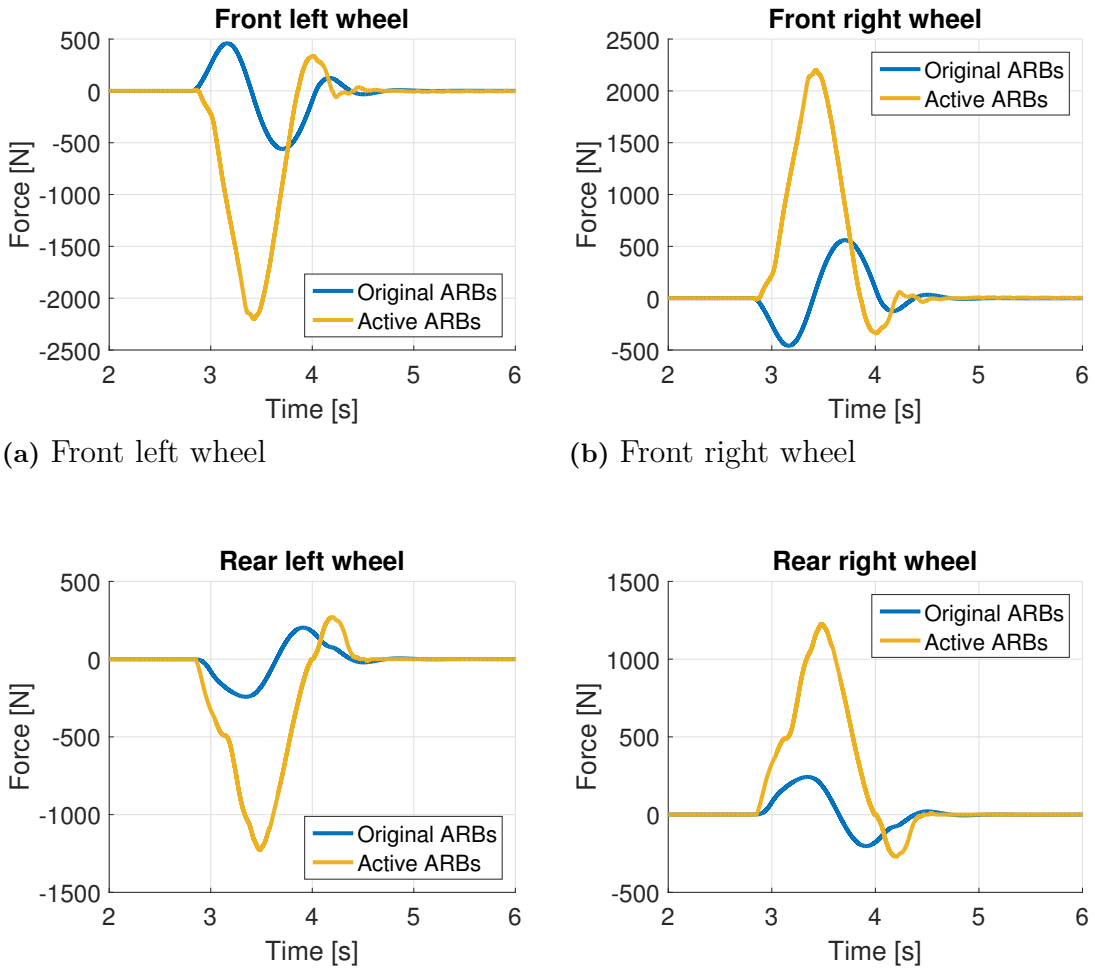

(a) Front left wheel

(b) Front right wheel

(c) Rear left wheel

(d) Rear right wheel

Figure 6.3: Wheel forces created by the original ARBs and the active ARBs in a single sided cosine wave test with test speed 60km/h.

6.1.1.2 Speed dependency

Test speed in the single sided cosine wave test is seen to have an effect on the performance of the active ARBs. Figure 6.4a shows the roll angle as a function of time for a test speed of 30km/h. It can be seen here that the roll angle is reduced and that the small roll overshoot is removed. Figure 6.4b shows the results for a test speed of 90km/h. It can be seen here that the roll angle is reduced by the active ARBs but that the roll overshoot is not eliminated. This is due to a combination of lack of roll damping, long response time and limitation of torque output from the active ARBs. This indicates that a speed dependent tuning of the roll damping controller would be beneficial.

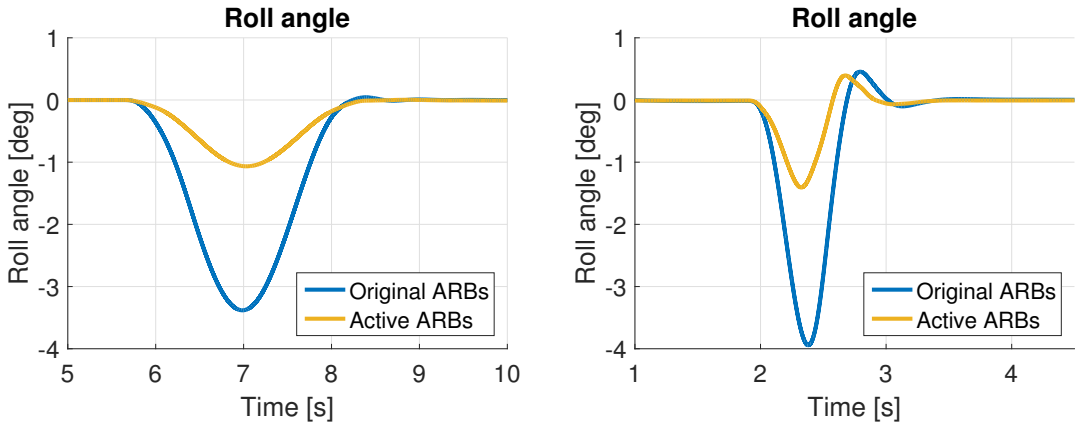

(a) 30 km/h **(b)** 90 km/h

Figure 6.4: Roll angle as function of time for a single sided cosine wave test with test speeds 30km/h (a) and 90 km/h (b).

6.1.2 Single sided ramp

Simulations of single sided ramp events are conducted to evaluate the performance of the active ARBs and the control strategy for high frequency road excitations.

6.1.2.1 Evaluation of the active anti-roll bar plant model

As introduced in section 2.5.1, the active ARB plant has an inbuilt controller which based on the required torsion angle and disturbances produces an output torque. In high frequency events, the response time of the active ARB is crucial and therefore simulations with a fixed reference torsion of zero i.e., a desired torque output of zero, are conducted to study the behaviour of the plant. The simulation results in terms of roll accelerations and vertical accelerations are compared to a vehicle with passive ARBs, as shown in Figure 6.5a and 6.5b respectively. The simulation results show that the active ARBs increases the amplitude of the roll acceleration and reduces the damping. The vertical accelerations shown in Figure 6.5b shows that the peak accelerations are slightly increased while the damping is unaltered. The conclusion drawn from this simulation is that the active ARB plant does not behave as expected and for this certain test it worsens the performance compared to passive ARBs.

However, it is important to remember the lack of accurate vertical tyre dynamics and that this result is only one test case. Hence, further investigations are needed to determine the active ARBs performance in high frequency road excitations.

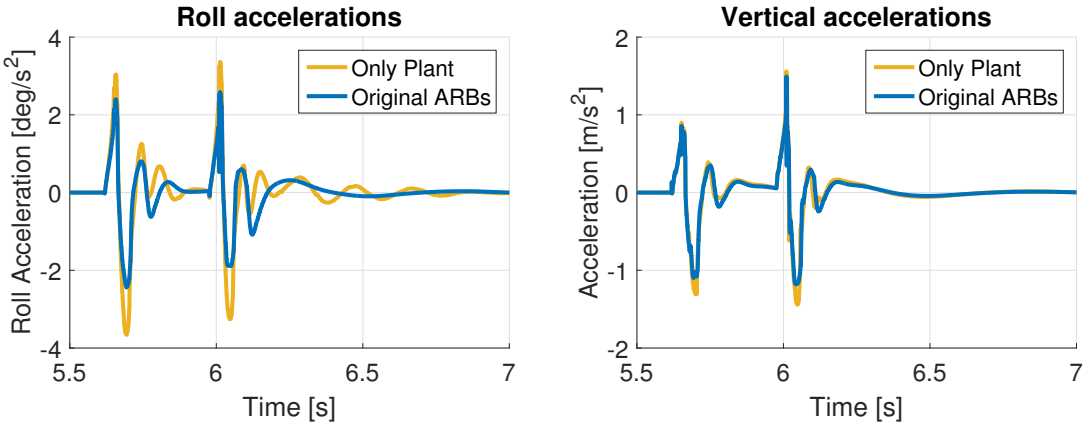

(a) Roll acceleration **(b)** Vertical acceleration

Figure 6.5: Roll acceleration (a) and vertical acceleration (b) as function of time for a single sided ramp test with only the internal controllers in the active ARBs.

6.1.2.2 Control strategy evaluation with ideal plant model

Due to the lack of accuracy in high frequency ride comfort simulations and the uncertainty regarding the plant model, focus is shifted to evaluation of the control strategy for high frequency road excitations. These simulations are conducted with an ideal plant model of the active ARBs which represents the ARBs as a simple stiffness without any non-linearity or phase delay. This is to focus solely on the control strategy, see results in Figures 6.6 and 6.7.

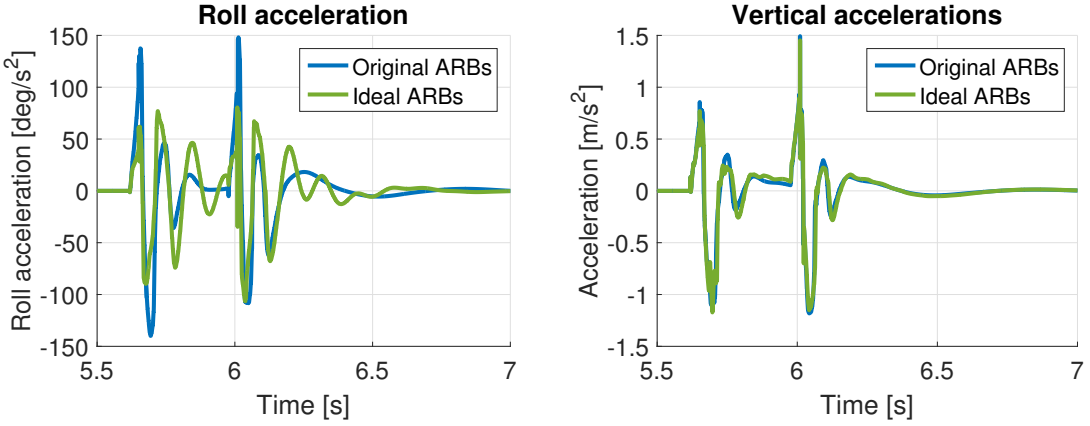

(a) Roll acceleration **(b)** Vertical acceleration

Figure 6.6: Roll acceleration (a) and vertical acceleration (b) as function of time for a single sided ramp test with an ideal active ARB plant model.

Figure 6.6a shows the roll accelerations for the ideal active ARBs with corresponding controller compared to the roll accelerations for a vehicle with the original ARBs. It can be seen that implementing the ideal ARBs reduces the peak roll accelerations but at the same time the damping is heavily reduced. The vertical accelerations of the vehicle body are more or less unaltered, see Figure 6.6b.

The wheel accelerations due to the ideal active ARBs and corresponding controller are shown in Figure 6.7. It is seen that the left wheels were more or less unaffected by the introduction of the active ARBs apart for some small oscillations in the acceleration of the rear left wheel when the front left wheel hits the ramp and vice versa. For the right hand side wheels, the active ARBs has a bigger impact. Here the active ARB induces new wheel accelerations as well as amplifies those seen for the vehicle with passive ARBs. Furthermore, a larger copying effect between the front left and rear right wheel is also seen.

(a) Front left wheel

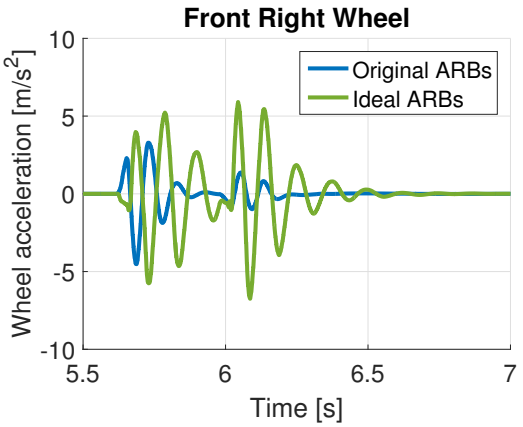

(b) Front right wheel

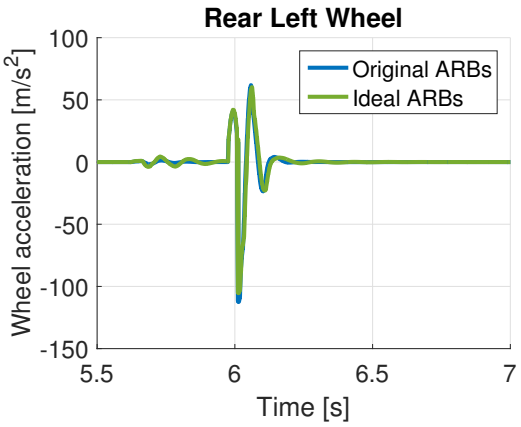

(c) Rear left wheel

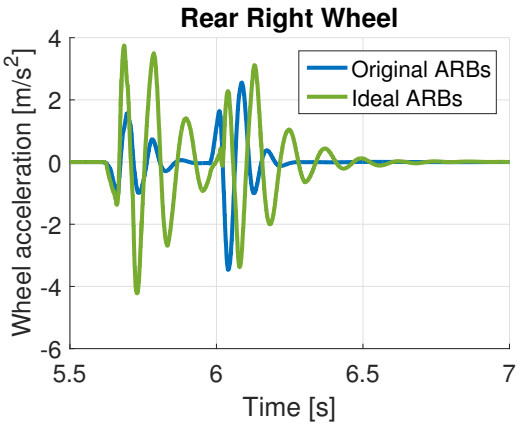

(d) Rear right wheel

Figure 6.7: Wheel accelerations for a vehicle with the original ARBs compared to a vehicle with ideal active ARBs for a single sided ramp test.

6.2 Handling

Three types of handling simulation tests are conducted, constant radius cornering, frequency response and sine with dwell. The purpose is to evaluate the effect of the active ARBs and the control strategy on vehicle handling.

6.2.1 Constant radius cornering

Constant radius simulations are conducted to evaluate the potential of active ARBs in terms of roll angle reduction and altering the understeer behaviour.

6.2.1.1 Roll reduction capabilities

Figure 6.8 shows the normalized roll angle as a function of normalized lateral acceleration with a roll angle reference of zero for different load transfer distributions. It is seen that the roll angle can be kept zero up to a maximum normalized lateral acceleration of 0.68 and that the roll angle reduction for the maximum lateral acceleration achieved is 68% of the original vehicle. Nevertheless, these numbers are only possible for the optimal load transfer distribution where the front and rear active ARB produces the maximum available torque at the same time. If the distribution is altered towards the front or rear axle, which in most cases it is expected to be, the maximum possible roll angle reduction is reduced. The yellow line shows the maximum roll angle reduction possible for a vehicle with all load transfer distribution on the front axle and green line is for the vehicle with all load transfer on the rear axle. From the simulations it is seen that all load transfer distribution on the front axle is setting the lower performance limit for the system. This implies that for any roll gradient in the area between the yellow and red line, any load transfer distribution is possible. If the desired roll gradient passes through the area created by the purple line and the yellow line restrictions are put on the load transfer distribution i.e., not any load transfer distribution is possible.

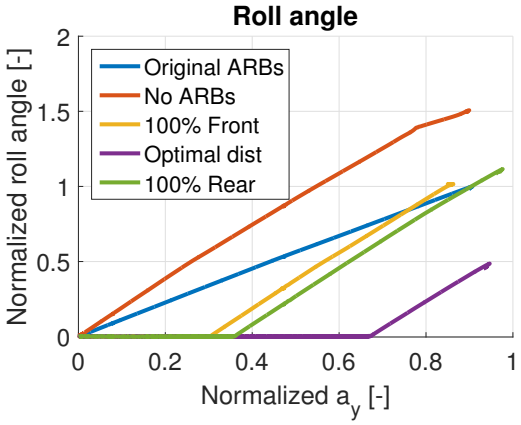

Figure 6.8: Normalized roll angle as a function of normalized lateral acceleration for different load transfer distributions.

Figure 6.8 shows the performance boundaries of the system. Within these boundaries, a wide range of roll gradients can be specified. To illustrate this Figure 6.9 shows a roll gradient using the existing vehicle's load transfer distribution with a smoothened out transition from a zero roll gradient to the roll gradient of the vehicle without ARBs. This way, the maximum roll reduction is more closely achieved for the given load transfer distribution without having a harsh change in roll gradient. This smoothened transition is expected to be better perceived by drivers.

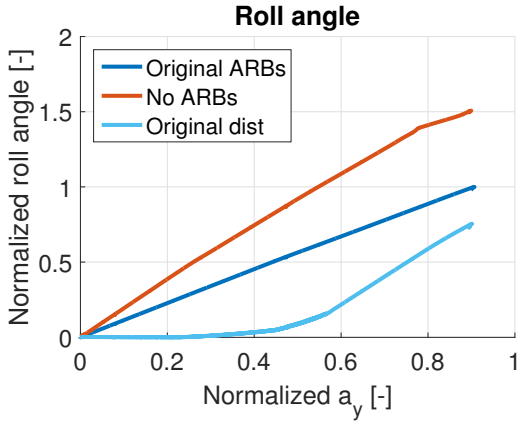

Figure 6.9: Normalized roll angle as a function of normalized lateral acceleration for an arbitrary roll gradient designed to maximise roll reduction using the original vehicle's load transfer distribution.

6.2.1.2 Handling capabilities

In order to understand the handling potential of active ARBs, the study presented in section 4.2.1 with passive ARB is repeated. To get the extreme distribution ratios, only one ARB is used at a time and the handling characteristics are compared to results obtained with passive ARBs.

It can be observed from Figure 6.10 that active ARBs are capable of providing a wider band of handling behaviours by allowing more or less understeer in comparison to a vehicle with passive ARBs. However the potential shown here is when the maximum amount of roll stiffness is provided, i.e. the roll angle of the vehicle is kept as close to zero as possible. This requirement actually helps the active ARBs in achieving the required handling behaviour as more torque is available for distribution. However, this is only true when cornering at low lateral accelerations. At higher accelerations, distribution requirements limit the roll reduction capability as both active ARBs cannot simultaneously operate at maximum torque limits.

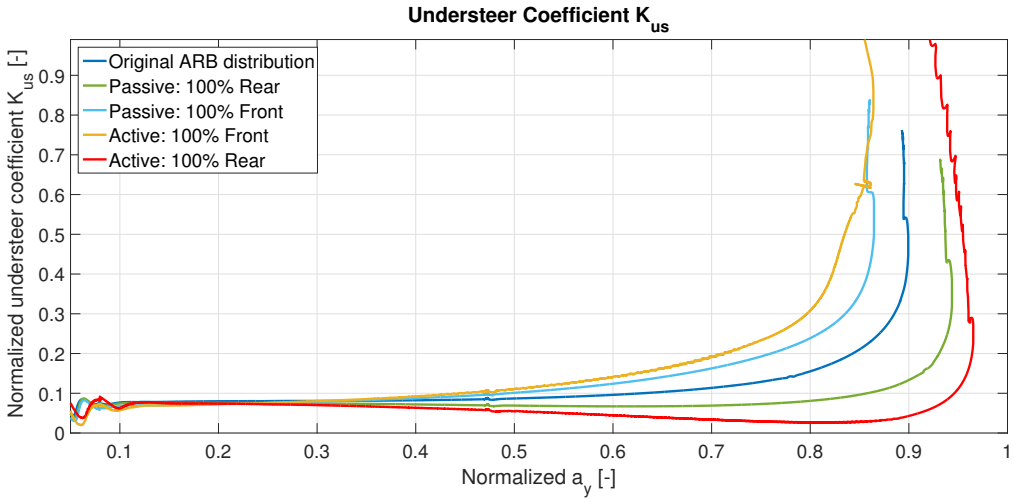

Figure 6.10: Handling characteristics for different stiffness distribution

6.2.2 Frequency response

Figure 6.11 shows the results, in terms of normalized roll angle gain and corresponding phase angle, obtained from frequency response simulations in accordance with section 3.2.2. The purpose with these simulations is to study the interaction between the developed controllers and the active ARB plant model. The simulation results shows the behaviour of the vehicle with the original ARBs and with active ARBs controlled by the roll damping controller. Two simulations are performed for active ARBs, one uses an ideal ARB plant model, i.e. a simple stiffness, and one uses the real ARB plant model. Furthermore, the normalisation factor used is the steady state roll angle gain of the vehicle with the original ARBs.

In Figure 6.11a it can be seen that for low frequencies, i.e. steady state, the roll damping controller reduces the steady state roll angle gain compared to the original vehicle, using both plant models. Also the phase angle seen, in Figure 6.11b is the same for both plant models for low frequencies. For high frequencies a deviation between using the real plant model and the ideal model is seen. There is a resonance between the plant model and the controller around 4Hz which does not occur with the ideal plant model. This is potentially due to the bandwidth of the plant model but this still needs to be studied further. Furthermore, a coherence analysis of the simulation results with the real plant model shows that the coherence is generally low, around 80% for the entire frequency range. Hence, these results are not considered to the reliable. Therefore, the rest of the frequency response simulations are conducted with the ideal plant model as the interaction between the roll damping controller and the plant model needs to be studied further before any conclusion can be drawn from simulation with the real active ARB plant model.

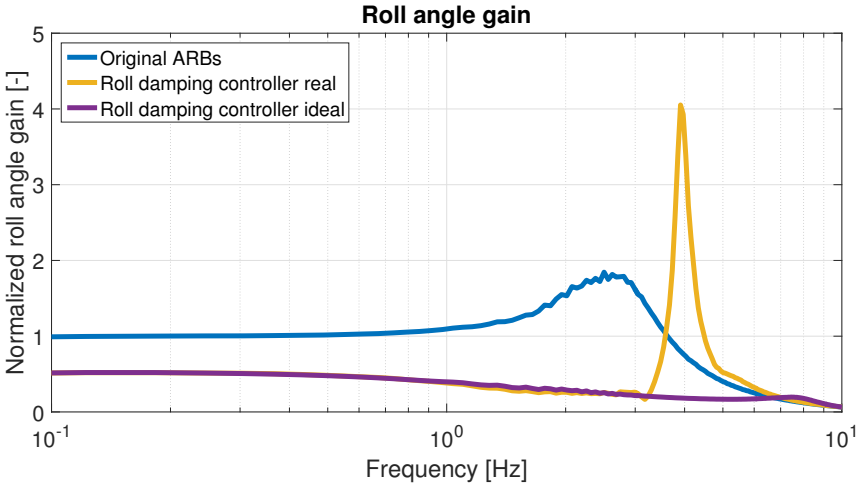

(a) Roll angle gain

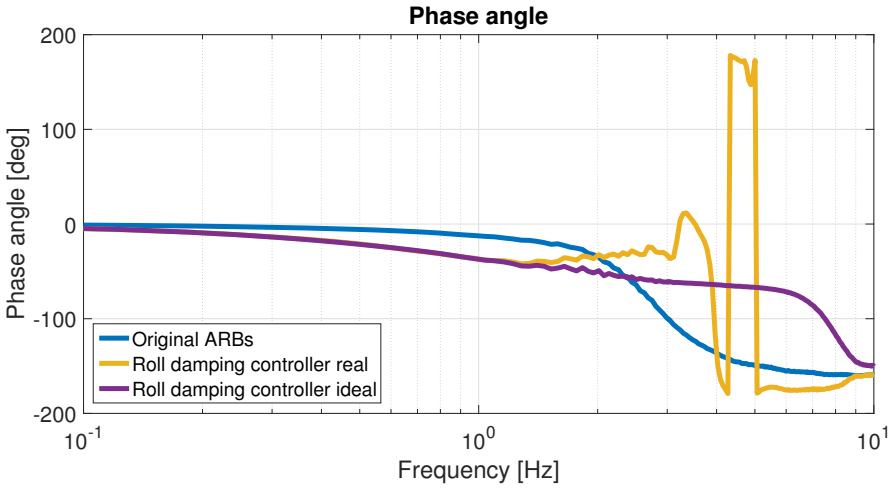

(b) Phase angle

Figure 6.11: Normalized roll angle gain (a) and phase angle (b) from frequency response simulations using the roll damping controller with a ideal plant model and with the real plant model in comparison to the original vehicle.

Further simulation results from applying the feed forward controller and the roll angle controller together with the roll damping controller are shown in Figure A.6 in Appendix A. These simulations highlight a problem with the strategy of using the original vehicle as reference for the feed forward and the roll angle controller in comparison to the roll damping controller which uses a absolute reference of zero. This makes the controllers strive towards different objectives for frequencies around the roll eigenfrequency. The feed forward and the roll angle controller will try to maintain a proportion of the roll angle gain of the original vehicle according to the roll reference gain. This also implies that it tries to maintain the eigenfrequency of the original vehicle. Whereas, the roll damping controller strives at minimising the roll rate and hence increasing roll damping. Hence, the rest of the frequency response simulations in this section are conducted only using the roll damping controller.

Figure 6.12 shows the impact of the I-part and the P-part of the roll damping controller on the vehicle's roll angle gain and phase angle in comparison with the complete PI-controller. Comparison is made for both, the original vehicle and the same vehicle without ARBs. The roll angle gain in Figure 6.12a shows that the I-part of the controller is as expected from theory, reducing the steady state roll angle gain, shifting the eigenfrequency to higher frequencies and reducing the roll damping. Comparing the curve for the I-part and the roll damping controller it can be seen that the I-part is solely determining the roll behaviour for low frequencies i.e., steady state. The P-part determines the high frequency behaviour around the roll eigenfrequency i.e., the roll damping, as expected according to theory. The effect on phase angle is seen in Figure 6.12b. The I-part decreases the phase angle giving a more responsive behaviour with less time delay between the peak lateral acceleration and the peak of roll angle. Whereas, the P-part increases phase shift.

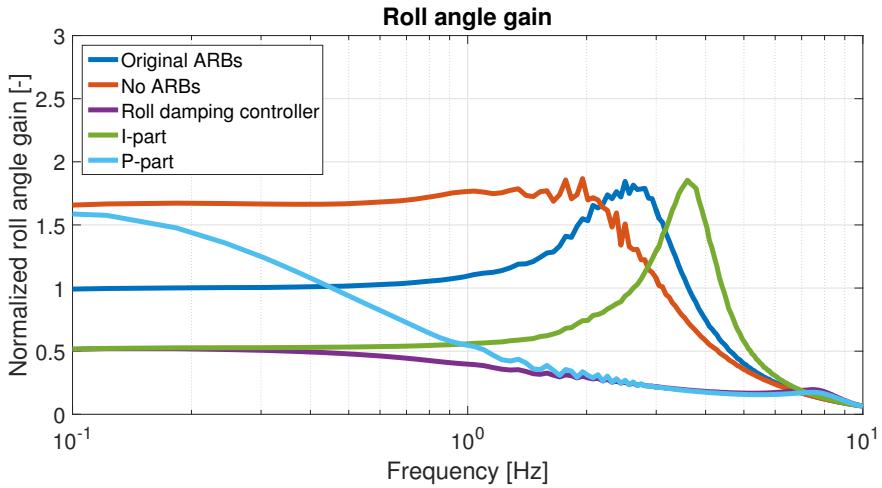

(a) Roll angle gain

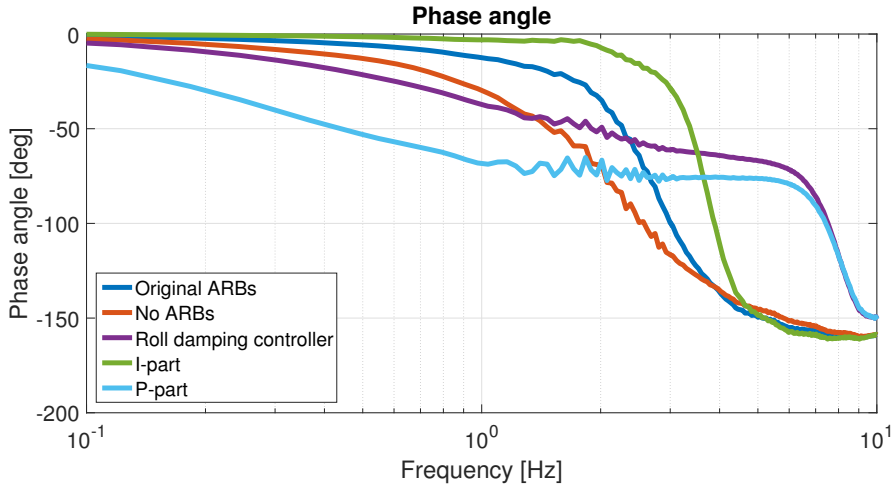

(b) Phase angle

Figure 6.12: Normalized roll angle gain (a) and phase angle (b) from frequency response simulations using the roll damping controller with an ideal and real plant model in comparison to the original vehicle and a vehicle without ARBs.

Using the results in Figure 6.12 the tuning of the roll damping controller can be altered to achieve the desired behaviour depending on vehicle type and characteristics. The original roll damping controller is a compromise made to make the controller work in all studied test scenarios and this resulted in an over-damped roll behaviour. Lowering the P-part slightly in the controller gives the roll behaviour seen in 6.13. It can be seen that vehicle is close to critical damping which gives a predictable behaviour of the vehicle as the roll angle gain is constant until the region of the roll eigenfrequency of the vehicle where it starts to reduce, see Figure 6.13a. The phase angle in Figure 6.13b is reduced for lower frequencies compared to the controller with a higher P-part. The phase angle for the critically damped system is close to the original vehicle up until about 2Hz after which the phase angle for the original vehicle increases faster.

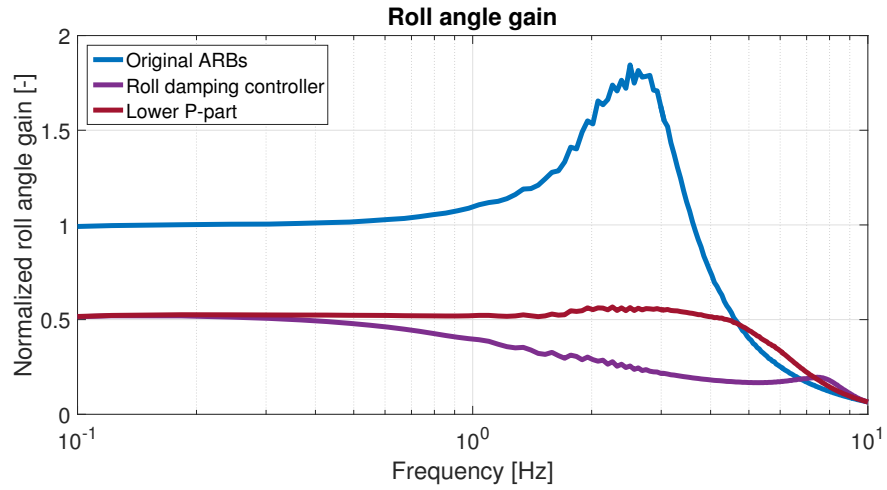

(a) Roll angle gain

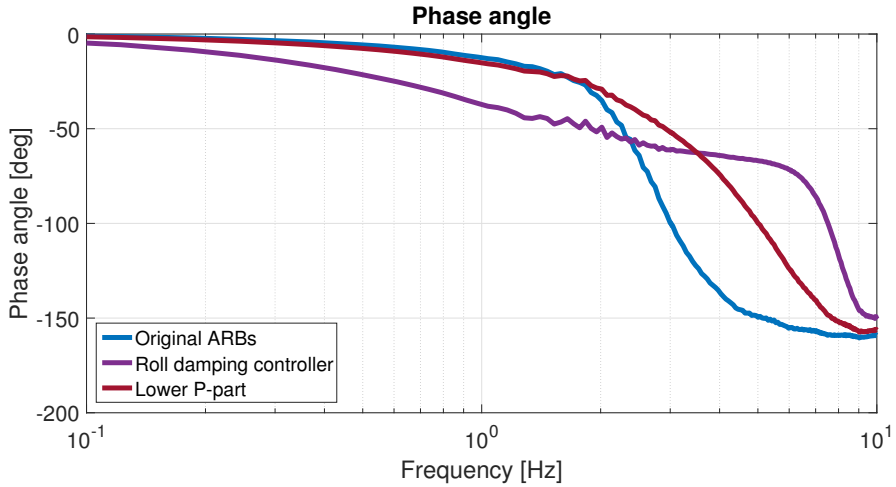

(b) Phase angle

Figure 6.13: Normalized roll angle gain (a) and phase angle (b) from frequency response simulations using the original roll damping controller and a roll damping controller with a lower P-part in comparison with the original vehicle.

Figure 6.14 shows the resulting yaw behaviour, in terms of the normalized yaw rate gain and corresponding phase angle, from implementing the original roll damping controller with the original distribution, with all load transfer on front and on the rear axle. The yaw rate gain in Figure 6.14a shows that all three distributions increase the steady state yaw rate gain which as explained in section 4.2.2 could be because of the roll understeer behaviour of the vehicle. Furthermore, all three distributions achieve the same roll behaviour and hence all differences between the three are solely due to the load transfer distribution. Hence, it can be concluded that having all load transfer distribution on the front axle decreases the yaw rate gain in steady state while moving it rearwards increases the yaw rate response. This is in contradiction to what was observed in section 4.2.2 where the load transfer were not seen to have any effect on the yaw behaviour in steady state. The reason for this is the increased load transfer on the respective axles as the roll reduction here is higher. Hence also the load transfer is higher and the tyres are operating outside the cornering stiffness linear range. For frequencies above and close to the yaw rate eigenfrequency the difference between the three distributions is decreased indicating that the load transfer distribution does not influence the high frequency yaw behaviour of the vehicle at low lateral accelerations. Furthermore, the phase angle in Figure 6.14b is seen to be unaffected by the load transfer distribution.

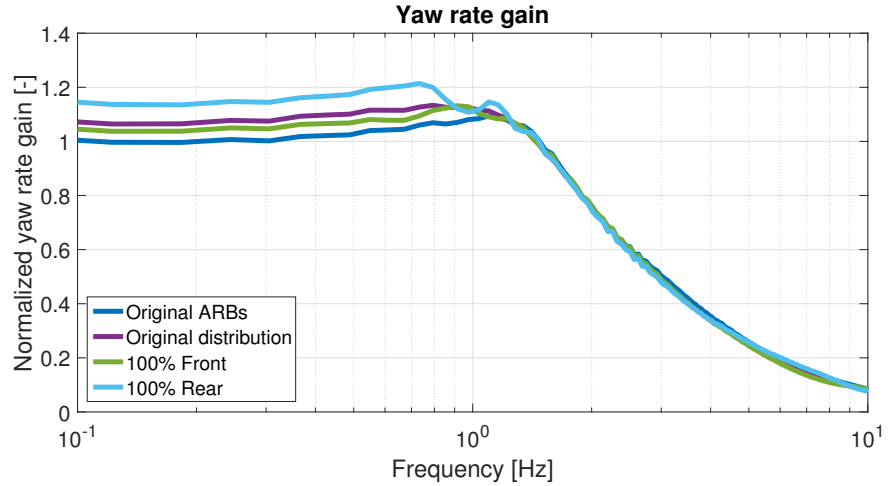

(a) Roll angle gain

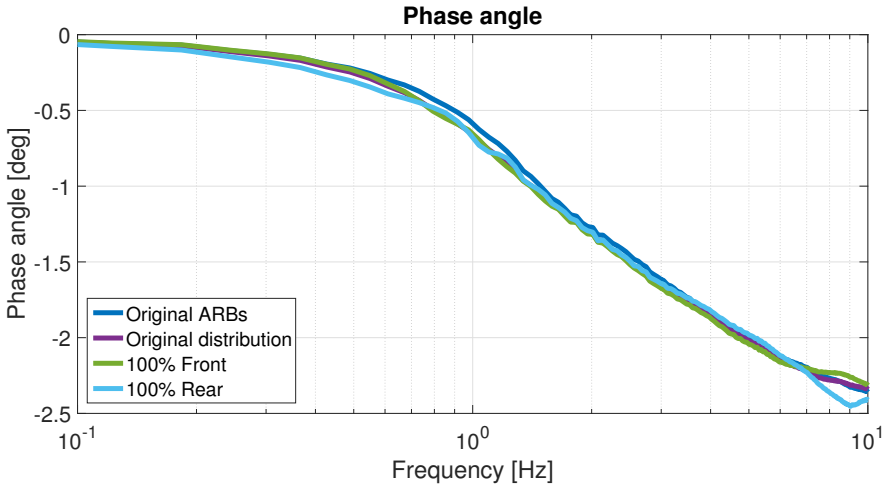

(b) Phase angle

Figure 6.14: Normalized yaw rate gain (a) and phase angle (b) from frequency response simulations using the roll damping controller with different load transfer distributions in comparison with the original vehicle.

6.2.3 Sine with dwell

Sine with dwell simulations are conducted to evaluate the performance of the control strategy in transient manoeuvres in the nonlinear range. For actual results and metric data, refer Appendix B.3.

6.2.3.1 Handling performance

Study of the handling performance with active ARBs requires the usage of the distribution controller. The results are compared to passive ARB as presented in Figures 6.15 and 6.16.

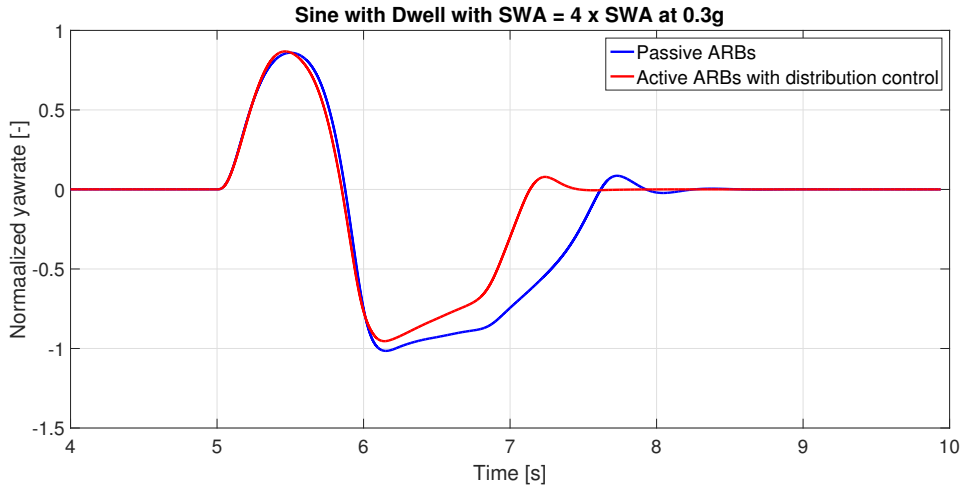

Figure 6.15: Normalized yaw rate with passive and active ARBs for a SWA=4xSWA at 0.3g.

It can be observed in Figure 6.15 that for the given understeer reference, peak yaw rate during dwell phase is reduced and yaw damping is also visibly better. This is also reflected in the metrics. With the given improvement in stability and yaw performance, the same manoeuvre is repeated with higher steering angle, see Figure 6.16.

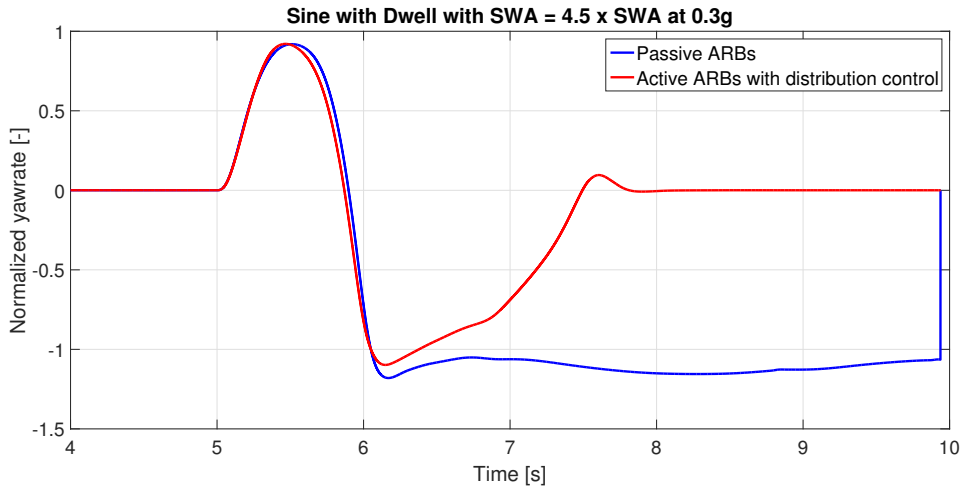

Figure 6.16: Normalized yaw rate with passive and active ARBs for a SWA=4.5xSWA at 0.3g.

It is observed from Figure 6.16 that the vehicle with passive ARBs cannot complete the manoeuvre with larger steering amplitude. This is because ARBs are unable to provide sufficient lateral stability. On the other hand, active ARBs along with distribution control allow the vehicle to complete the manoeuvre successfully and within the defined metric limits. It is a clear depiction of vehicle's improved handling capabilities.

6.2.3.2 Roll performance

For studying the roll reduction capability of active ARBs during a sine with dwell manoeuvre, roll angles are compared with those obtained with passive ARBs, as seen in Figure 6.17.

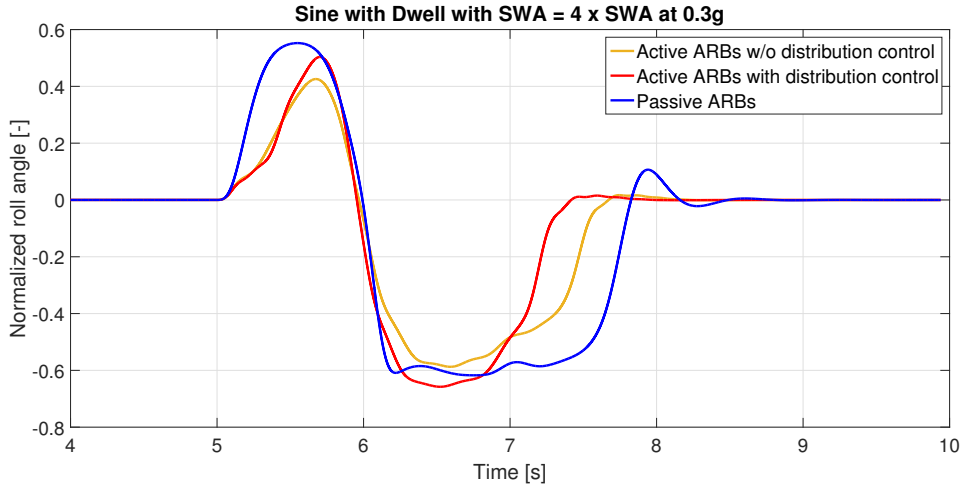

Figure 6.17: Normalized roll angle with passive and active ARBs for a SWA=4xSWA at 0.3g.

It can been seen from Figure 6.17 that using active ARBs without distribution control yields the best performance in terms of reduction of peak roll angles. The roll damping is also significantly better towards the end of the manoeuvre compared to passive ARBs. When using distribution control, the roll reduction capability of active ARBs is compromised at the cost of better roll damping as the vehicle returns to the original state much faster and in a smoother fashion. Figure 6.18 presents the result from the test with the increment in input steering angle i.e., 4.5 times steering angle at 0.3g.

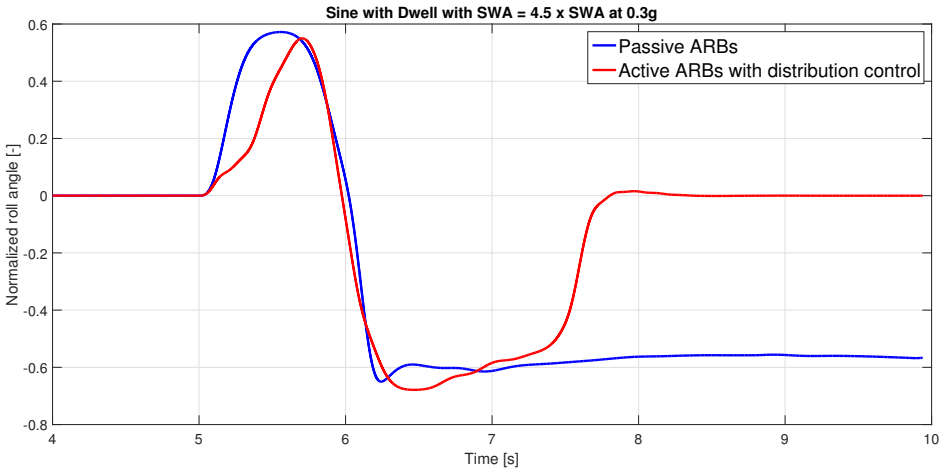

Figure 6.18: Normalized roll angle with passive and active ARBs for a SWA=4.5xSWA at 0.3g.

It is observed from Figure 6.18 that by using active ARBs with distribution control, the vehicle is now able to successfully complete the manoeuvre with higher steering inputs and without any significant compromise on roll reduction capability compared to with passive ARBs.

7
Discussion

The potential of using active ARBs to improve ride comfort in low frequency road excitations such as the single sided cosine wave is considered to be good. Potential was seen in reducing the peak roll angle due to the road excitations for all test speeds and potential in increasing roll damping was seen for 30 and 60km/h. Hence the current control strategy of roll damping is considered to be sufficient in these situations. The roll damping seems to be sensitive to the tuning of the controller as well as the capacity of the active ARBs in terms of maximum torque and response time. As the roll overshoot was not damped out by the current controller tuning in combination with the active ARB plant model at high speeds, it can be concluded that a speed dependent tuning of the roll damping controller is probably needed to achieve the best possible roll damping performance.

For high frequency road excitations, the true performance of the active ARBs could not be reflected in this thesis. The results obtained for the single sided ramp showed that the active ARB plant reduced the ride comfort of the vehicle and the same can be said for the current roll damping control strategy. Firstly, a new control strategy is needed for high frequency road excitations. Increasing roll damping is not a suitable control strategy for such cases. It is instead recommended to focus on the vertical accelerations of the wheels by implementing for example, a skyhook controller. It should be noted that control of individual wheels is hard using active ARBs, as the force applied to the left wheel will correspond to a force on the right wheel in the opposite direction. Therefore, this is not a straightforward solution and a combination of active dampers and active ARBs might be the solution here. Secondly, as per the active ARB supplier, ARBs should be able to increase ride comfort by managing high frequency road excitations. As explained before, one possibility for the results obtained is that the system is not implemented in the right way. A major possible reason could also be the lack of proper tyre vertical dynamics which are critical for secondary ride analysis. Furthermore, the stiffness of the ARB itself is important for these kind of evaluations and the influence of this factor has not been covered in this thesis. The secondary ride comfort simulations with passive ARBs showed a reduction of the RMS values of vertical acceleration due to road irregularities by reducing the ARB stiffness. It is assumed that during straight line driving it would be possible with active ARBs as well. The end effect on ride comfort will obviously depend on the active ARB's inbuilt controller. The personal reflection of the authors is that, even though the results so far have shown a negative impact on the secondary ride comfort from the active ARBs, an improvement compared to passive ARBs is thought to be achievable.

Roll reduction in steady state cornering shows great potential in simulations, even though a trade-off between roll reduction and influencing vehicle handling exists. As mentioned already, all simulations have been conducted with the current XC90's suspension geometry and this is the reason for the front axle to be the limiting factor. The combination of arm length of the ARB and motion ratio is less beneficial in the front, hence the performance of the front active ARB will be lesser, see equation 2.2. When using active ARBs, this difference between the front and rear suspension geometry is thought to be of great importance. A more beneficial motion ratio and arm length in the front would increase the potential in roll reduction and hence also reduce the trade-off between roll reduction and influencing yaw behaviour of the vehicle.

The control strategy used in steady state cornering is observed to work well but it is also shown to induce unwanted behaviour in frequency response simulations. The choice of using the passive vehicle as reference works in steady state cornering but to be able to increase roll damping this strategy was shown to be a bad choice. Furthermore in steady state cornering the dynamic part of the transfer function in 2.8 is not used. Hence a good solution to get a better control strategy in all aspects would be to only use the static part of the transfer function. Furthermore, the next conflict seen was the roll damping controllers I-part, as it strives to achieve zero roll angle no matter what the reference roll angle is. This cannot be used during cornering and hence a more advanced logic choosing which controller that should be used is recommended.

Frequency response simulations once again confirmed that the roll angle reduction in steady state has potential but also that active ARBs can increase roll damping and even make the system over damped if that would be desired. Furthermore, these simulations also showed that a different tuning of the roll damping controller is probably desired here, compared to what is desired for increasing ride comfort. However, this is with the assumption that the actual active ARB together with the controller does not create a resonance behaviour around 3-5Hz. Even if this would be the case there is still potential of affecting the roll behaviour up to 3Hz as both plant models, in Figure 6.11, showed the same behaviour up to this frequency.

Active ARBs showed great potential in influencing handling capabilities of a vehicle. Evaluation of the handling performance in steady-state conditions using passive ARBs showed a good working range that could be theoretically obtained. Moving stiffness completely to front and rear axle changed the handling characteristics to quite an extent, especially at high lateral accelerations. For the development of the distribution controller for active ARBs, while the bicycle model provided easy simplification, most of the non-linearities are instead handled by the SMC controller which can make the control strategy a bit inefficient. Some ad-hoc solutions have to be implemented to make the control strategy work e.g. avoiding the use of sign function within the SMC and using 'unit delay' blocks to identify zero crossover. Distribution is then made directly proportional to the output of the controller instead of implementing tyre stiffness curves which would provide more accurate data on the relationship between load transfer and lateral forces, especially in the non-linear range.

The handling behaviour shown in the frequency response simulations suggested that for lateral accelerations around $4m/s^2$ the steady state yaw rate gain increases with reduced roll independently of the load transfer distribution. This could be due to that the reduction in roll angle reduces the impact of roll understeer and hence makes the vehicle less understeered. However further investigations are needed to conclude that this is the actual and only cause. Furthermore, the load transfer distribution effects the yaw behaviour but not enough to overcome the effect of reduced roll angle. Hence having all load transfer on the front axle still makes the vehicle more oversteered than the original vehicle. However, comparing these results with the results from steady state cornering for higher lateral accelerations, the reduction in roll angle plays less importance. For higher lateral accelerations, the load transfer distribution is having larger influence and hence overcomes the effect from the reduced roll angle.

Sine with dwell manoeuvres were simulated to evaluate the performance in non-linear ranges. A reference understeer curve was defined which cannot be completely validated and is based on the capability of the active ARB in steady-state conditions. As the nominal requirement on SUVs are to create understeer at high lateral accelerations, for a given understeer reference, lower yaw rates were achievable with improved yaw and roll damping. As also reflected during steady-state evaluations, limitations with the front axle suspension creates a trade-off between the improvement in roll and lateral stability.

Because of the trade-off, an intelligent strategy is required to be in place that prioritises the requirements. For example, the extent of sacrifice that can be made on roll angle to achieve the desired distribution. The current strategy of not allowing the distribution ratio to decrease above a certain lateral acceleration value is not likely to be a robust strategy in real-world conditions.

8

Conclusions and Future work

The objective of investigating how active ARBs can be used to improve customer value has been fulfilled by developing a control algorithm and evaluating it's performance in terms of handling and ride comfort. Strategies developed for controlling roll stiffness and the distribution were able to reflect the potential active ARBs can provide in improving the handling and ride behaviours. The approach for merging these controllers in an effective way was critical to the active ARB's performance. Major potential of active ARBs is seen in roll reduction and manipulating the understeer behaviour at high lateral accelerations. In ride comfort evaluations, active ARBs are able to isolate the vehicle from low frequency road excitations and eliminating the roll overshoot at the same time. The performance for high frequency road excitations still needs to be investigated further. In handling evaluations, active ARBs exhibit a range of possibilities. However, for low lateral accelerations (upto 4m/s^2), active ARBs show negligible effect on high frequency yaw behaviour. Evaluation of active ARBs for non-linear transient conditions show a significant improvement in improving the on-limit handling stability of the vehicle with a considerably reduced trade-off between handling and ride performance.

An important conclusion made during the thesis is the high dependency of the performance of active ARBs on the suspension design. The wide range of vehicle behaviour achievable using active ARBs suggest that they are a good tool to differentiate between different driving modes in a vehicle and allow the driver to tailor the vehicle's driving dynamics.

Further detailed investigations regarding the active ARB concept are required in terms of controller robustness, performance and limitations. The recommended future activities are:

- Obtain deeper understanding and knowledge regarding the active ARB plant model.
- Establish what is the subjectively desired vehicle behaviour in terms of roll gradient, understeer behaviour and steering feel. A vehicle simulator based study could be suitable.
- Study the performance of active ARBs for manoeuvres with simultaneous requirements on ride and handling.
- Investigate the effects of active ARBs on steering feel.
- Determine the performance of active ARBs for high frequency road excitations.

Bibliography

[1] Bernd, H., Ersoy, M. Chassis Handbook. Springer Fachmedien Wiesbaden GmbH, 2011.

[2] Nastasić, Ž., Deák Jahn, G. The Citroën Technical Guide.

[3] Ohta, Y., Kato, H., Yamada, D., Fukino, T., Nobayama, E., Buma, S. Development of an Electric Active Stabilizer System Based on Robust Design. SAE World Congress. Detroit, Michigan: SAE Technical Paper 2006-01-0758, 2006

[4] Toyota Motor Corporation, 2017. [Online]
Avalible: http://www.toyota-global.com/company/history_of_toyota/75years/data/automotive_business/products_technology/technology_development/chassis/index.html

[5] Straßberger, M., Guldner, J., BMW's Dynamic Drive: An Active Stabilizer Bar System. IEEE Control Systems Magazine, 2004.

[6] Griffin, M. J. Handbook of Human Vibration. Southampton, Academic press, 1990.

[7] ISO 2631-1. International standard - Mechanical Vibration and Shock - Evaluation of Human Exposure to Whole-body vibration - Part 1.
International Organization For Standardization, 1997.

[8] Dieckmann, D. A Study of Vibration on Man. Ergonomics, 1958, p.347-355.

[9] Guglielmino, E., Sireteanu, T., Stammers, C.W., Ghita, G., Giuclea, M. Semi-active Suspension Control. London, Springer, 2008.

[10] Senthil Kumar, K., Pal, S., Sethi, R. C. Objective Evaluation of Ride Quality of Road Vehicles. SAE Technical Paper 990055, 1999.

[11] Ibicek, T., Thite, A.N. Quantification of Human Discomfort in a Vehicle Using a Four-post Rig Excitation. Journal of Low Fequency Noise, Vibration and Active Control, 2012, Vol. 31 No. 1 , p.29-42.

[12] Koumura, S., Ohkita, T. Ride Comfort Evaluation through Analysis of Roll and Lateral Vehicle Behaviours Due to Road Input. SAE Technical Paper 2008-01-0581, 2008.

[13] Wennerström, E., Nordmark, S., Thorvald, B. Compendium in Vehicle Dynamics, KTH Royal Institute of Technology, 2011.

[14] 10th Schaeffler Symposium April 3/4, Solving the Powertrain Puzzle, Schaeffler Technologies AG & Co. KG, 2014, pp. 398-400.

[15] Bentley 2017, Bently Bentayga Diesel: Effortless Driving With Peerless Luxury, Bentley Newsroom. [online]. Available: https://www.bentleymedia.com/en/newsitem/697

[16] Porsche, 2017, Dynamic Chassis Control Sport (PDCC Sport) including Porsche Torque Vectoring Plus (PTV Plus). [Online]. Available:

http://www.porsche.com/international/models/panamera/panamera/drive-chassis/porsche-dynamic-chassis-control-sport-pdcc-sport

[17] Audi, 2017, Audi SQ7 TDI: Driving Innovation, Audi MediaCenter. [Online]. Available: https://www.audi-mediacenter.com/en/press-releases/audi-sq7-tdi-driving-innovation-5730

[18] BMW Group, 2017, The new BMW 7 Series. [Online]. Available: https://www.press.bmwgroup.com/global/article/detail/T0221224EN/the-new-bmw-7-series

[19] Tingwall, E., 2017, "Deep Dive: Bentley Dynamic Ride Explained", Blog.caranddriver.com. [Online]. Available: http://blog.caranddriver.com/deep-dive-bentley-dynamic-ride-explained/

[20] Shtessel, Y., Edwards, C., Fridman, L., Levant, A. Sliding mode control and observation. New York, NY, USA: Birkhäuser, 2014.

[21] Canale M., Fagiano L., Ferrara L., Vecchio, C. “Vehicle yaw control via second order sliding-mode technique,” IEEE Transactions on Industrial Electronics, 2008, vol. 55, no. 11, pp. 3908–3916.

[22] ISO 4138, Passenger cars - Steady-state circular driving behaviour - Open-loop test methods. International Organization for Standardization, 2012.

[23] ISO 7401, Road vehicles - Lateral transient response test methods - Open-loop test methods. International Organization for Standardization, 2011.

[24] Forkenbrock, G.J., Elsasser, D.H., O’Harra, B.C., NHTSA’s Light Vehicle Handling and ESC Effectiveness Research Program, ESV june 2005, Paper Number 05-0221.

[25] Forkenbrock, G.J. and Boyd, P.L., "Light vehicle ESC performance test development", In proceedings of the 20th International Technical Conference on the Enhanced Safety of Vehicles, Lyon, France, June 18-21, 2007, Paper Number 07-0456.

A

Appendix

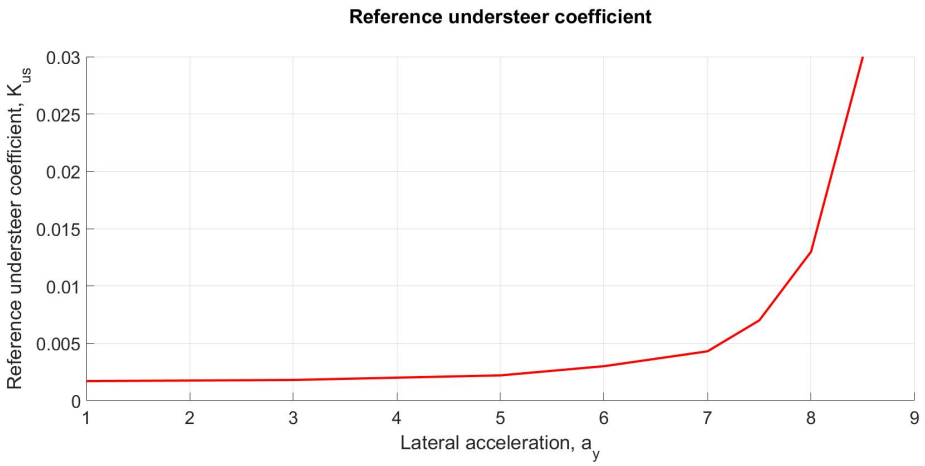

Figure A.1: Example reference for understeer coefficient

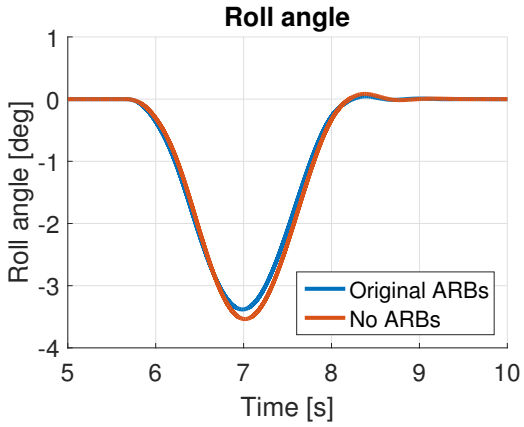

(a) Roll angle

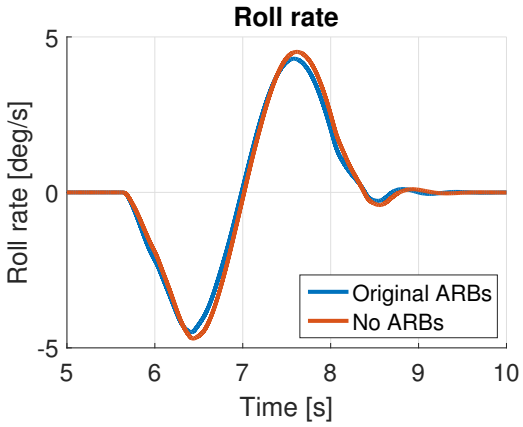

(b) Roll rate

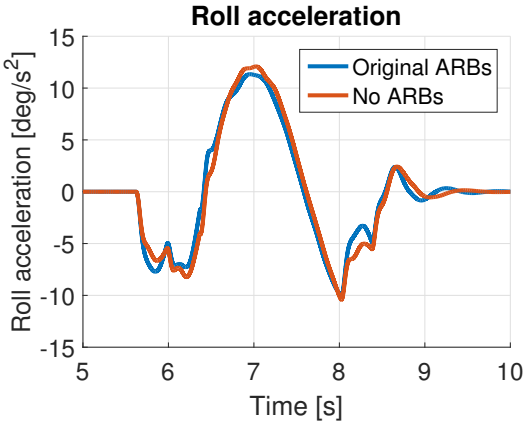

(c) Roll acceleration

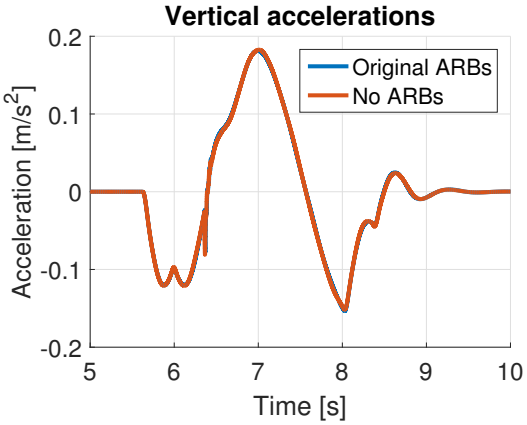

(d) Vertical acceleration

Figure A.2: Roll angle (a), roll rate (b), roll acceleration (c) and vertical acceleration (d) from a single sided cosine wave for a vehicle with and without ARBs for a test speed of 30km/h.

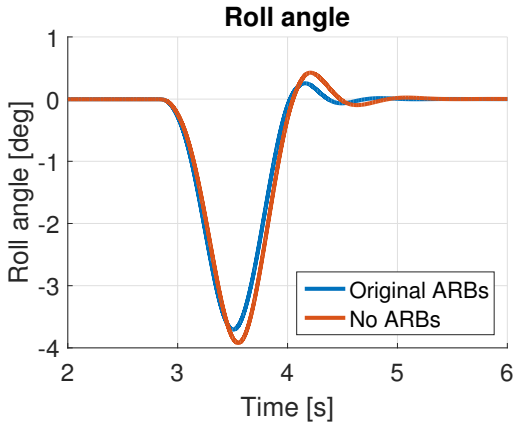

(a) Roll angle

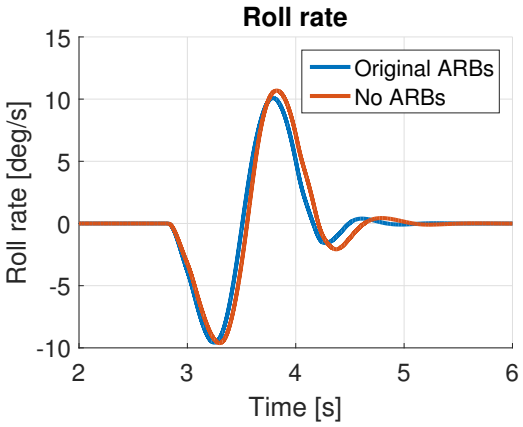

(b) Roll rate

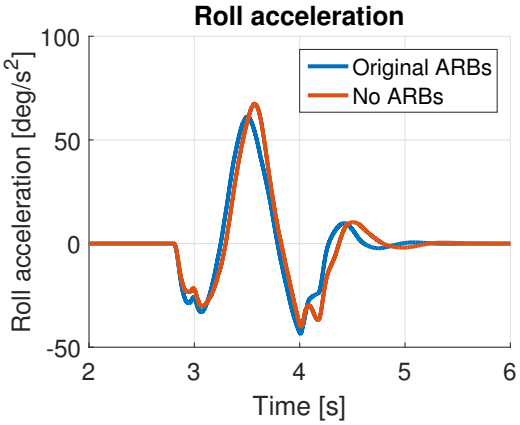

(c) Roll acceleration

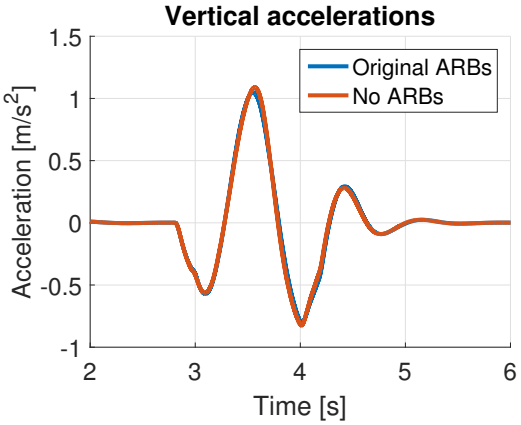

(d) Vertical acceleration

Figure A.3: Roll angle (a), roll rate (b), roll acceleration (c) and vertical acceleration (d) from a single sided cosine wave for a vehicle with and without ARBs for a test speed of 60km/h.

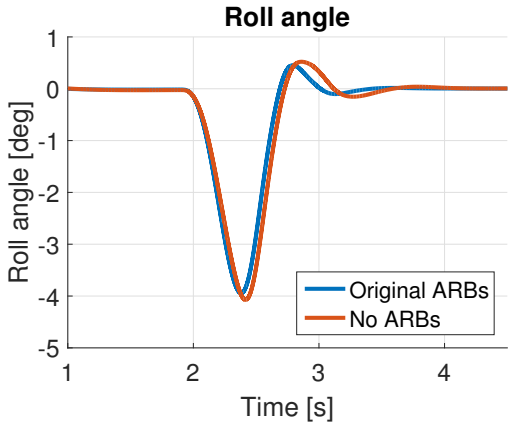

(a) Roll angle

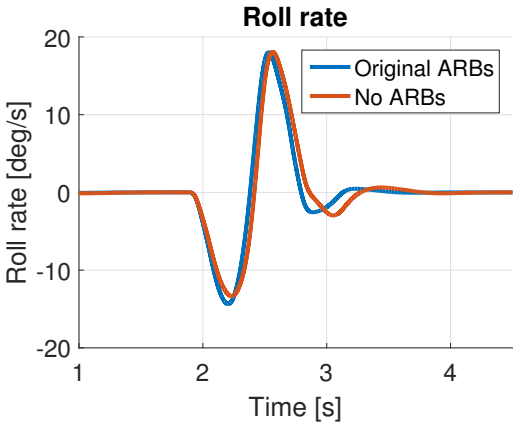

(b) Roll rate

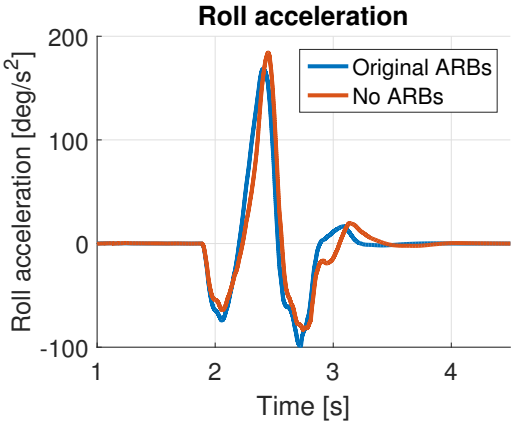

(c) Roll acceleration

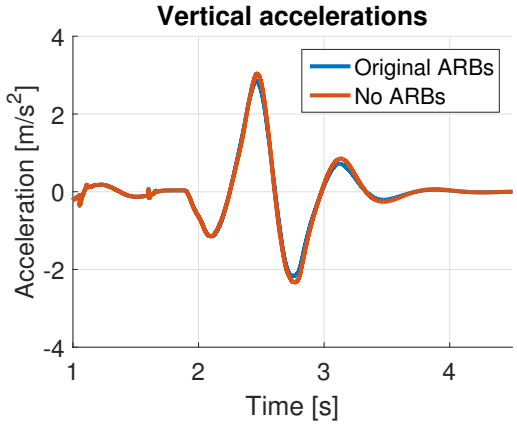

(d) Vertical acceleration

Figure A.4: Roll angle (a), roll rate (b), roll acceleration (c) and vertical acceleration (d) from a single sided cosine wave for a vehicle with and without ARBs for a test speed of 90km/h.

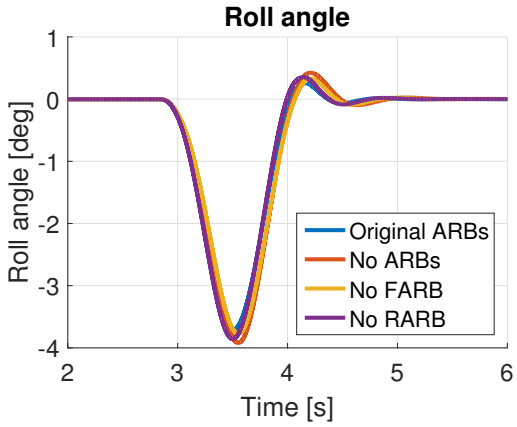

(a) Roll angle

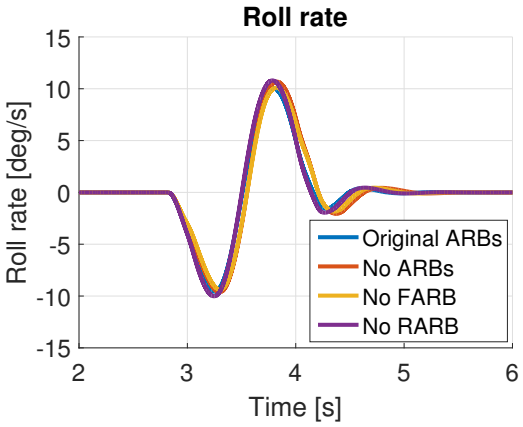

(b) Roll rate

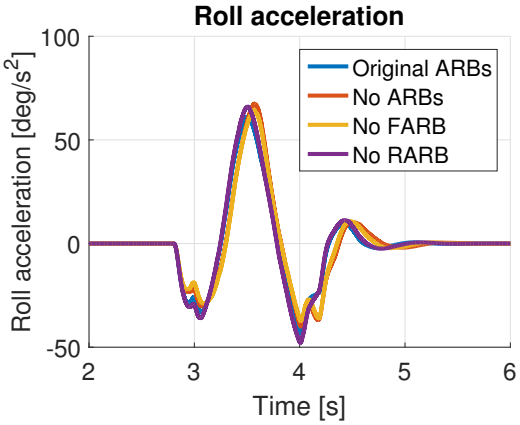

(c) Roll acceleration

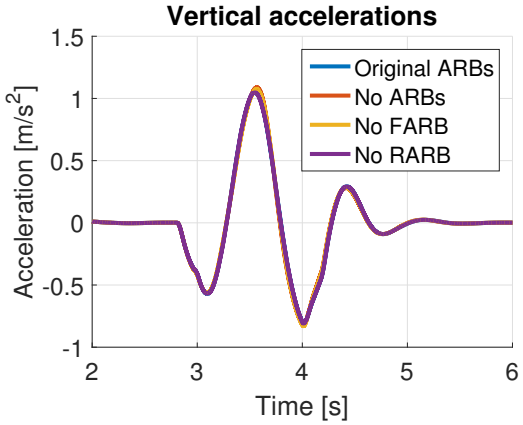

(d) Vertical acceleration

Figure A.5: Roll angle (a), roll rate (b), roll acceleration (c) and vertical acceleration (d) from a single sided cosine wave for a vehicle with ARBs, without ARBs, without front ARB and without rear ARB for a test speed of 60km/h.

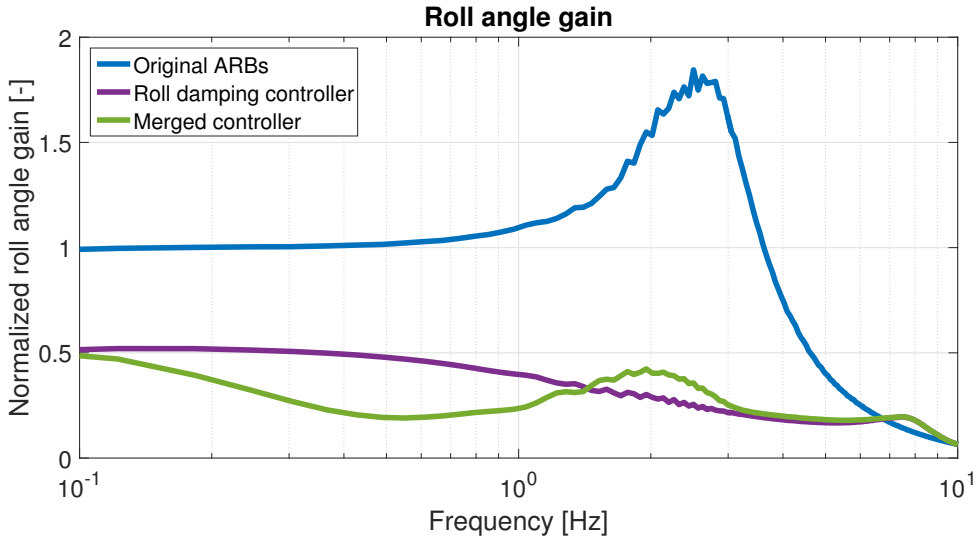

(a) Roll angle gain

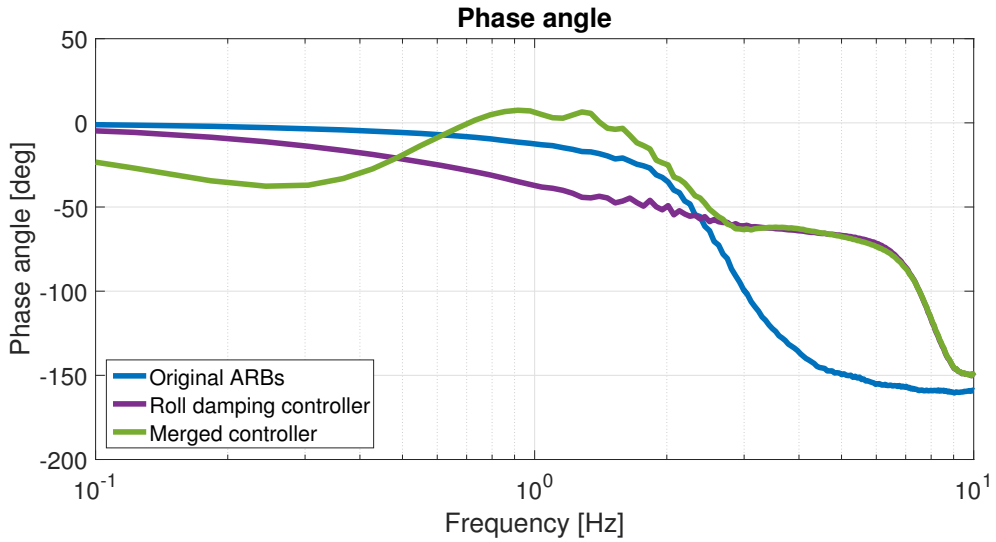

(b) Phase angle

Figure A.6: Roll angle gain (a) and phase angle (b) from frequency response simulations using active ARBs controlled by the roll damping controller and the entire controller in comparison to the original vehicle.

B

Appendix - Confidential

B.1 Simulations with passive anti-roll bars

This content is not available in the public report.

B.2 Control strategy

This content is not available in the public report.

B.3 Simulations with active anti-roll bars

This content is not available in the public report.